Electronic Supplementary Information (ESI)

Studies on influence of nuclearity of zinc(II) hemi-salen complexes on some pivotal biological applications

Bidyut Kumar Kundu,[a] Pragti,[a] Shaikh M. Mobin,[a] Suman Mukhopadhyay[a, b, *]

[a] Discipline of Chemistry, School of Basic Sciences, Indian Institute of Technology Indore, Simrol, Khandwa Road, Indore 453552, India

[b] Discipline of Biosciences and Biomedical Engineering, School of Basic Sciences, Indian Institute of Technology Indore, Khandwa Road, Simrol, Indore 453552, India.

* E-mail: suman@iiti.ac.in; Fax: +91 731 2361; Tel: +91 731 2438 735

Table of Contents

Section S1. Abbreviation used in this article

Entry	Significance	Entry	Significance
HL[1]	2-(((2-(diethyl amino)ethyl)imino) methyl) phenol	**XRD**	X-ray diffraction
HL[2]	o-methoxy-2-[[[3-(dimethylamino)-2,2-dimethyl propyl]imino] methyl]-phenol	**DAPI**	4′,6-diamidino-2-phenylindole
NMR	Nuclear magnetic resonance	**UV-Vis**	Ultraviolet-Visible
ESI-MS	Electrospray ionisation mass spectrometry	**E-coli**	Escherichia coli
FTIR	Fourier transformed infra-red	**AO**	acridine orange
CT-DNA	calf thymus deoxyribonucleic acid	**r.t.**	Room temperature
MTT	3-(4,5-dimethylthiazol-2-yl)-2,5-diphenyl tetrazolium bromide	**FL**	Fluorescence
λ_{max}	Absorption wavelength maxima	**h/ min**	hour/ minute

Section S2. Experimental section

Instrumentation

The measurements of pH have been done using a digital pH meter (TOSHCON INDUSTRIES PVT. LTD., AJMER). An AVANCE III 400 Ascend Bruker BioSpin machine was used to record ^{1}H and ^{13}C NMR spectroscopy at room temperature. Infrared (FTIR) spectra (range: 4000 to 500 cm^{-1}) was conducted on BRUKER TENSOR 27 instrument. Elemental analyses (C, H, N and S content) were performed with a MicroTOF-Q II mass spectrometer and ThermoFlash 2000 elemental analyzer. ESI-MS were carried out on Bruker-Daltonics. Absorption spectra were performed on a Varian UV-Vis spectrophotometer (Model: Cary 100). Fluorescence emission spectra were recorded at 25.0 ± 0.2 ºC on a Fluoromax-4p spectrofluorometer from Horiba JobinYvon (Model: FM-100) using a quartz cuvette with a path length of 2 cm. A HORIBA Jobin Yvon picosecond time-correlated single photon counting (TCSPC) spectrometer (model Fluorocube-01-NL) was used for recording PL decays. The samples were excited at 405 nm by a picoseconds diode laser (model Pico Brite-405L) at a magic angle of 54.7° by a photomultiplier tube (TBX-07C) to collect the PL decays. The instrument response function (IRF, FWHM ~140 ps) was recorded using a dilute scattering solution, and IBH DAS 6.0 software was used to analyze

the PL decays by the iterative reconvolution method. The goodness of the fit was judged by reduced χ-square (χ2) value. Hand held camera was used to take the photos of UV-chamber as well as in day light. A FEI quanta 200 3D dual beams having thermionic emission tungsten filament in the 3 nm range at 20 kV was introduced to record scanning electron microscopy (FE-SEM) images. Before analysis, the solid powders were deposited on a carbon-coated copper grid. The fluorescence images of cells were taken using an Olympus Confocal laser scanning microscopy with an objective lens (×40). AFM images have been captured in a Park NX10 system based on tapping non-contact mode. HRTEM images of catalysts were recorded using Carl zeiss Libra 200FE TEM microscope.

X-ray crystallography

The crystals were mounted onto quartz fibers and the X-ray diffraction intensity data were measured at 293 K with a Bruker APEX II diffractometer equipped with a CCD detector, employing Mo Kα radiation (λ = 0.71073 Å), with the SMART suite of programs.[1] All data were processed and corrected for Lorentz and polarization effects with SAINT and for absorption effects with SADABS. Structure solution and refinement were carried out with the SHELXTL suite and Olex2 programs.[2] Data were corrected for absorption effects using the multi-scan method (SADABS). The structures were solved by Patterson maps to locate the heavy atoms, followed by difference maps for the light, non-hydrogen atoms. All non-hydrogen atoms were refined with anisotropic thermal parameters. Crystal data and structural parameters are provided in Table 1.

Section S3. Experimental Methods

S3.1 DNA binding study

S3.1.1 Absorption spectral studies

The interaction between metal complexes and DNA were studied using electronic absorption method. Disodium salt of calf thymus CT-DNA was stored at 4 ºC. Solution of CT-DNA in the buffer 50 mM NaCl/ 5 mM Tris (pH 7.2) in water gave a ratio 1.9 of UV absorbance at 260 and 280 nm (A260/A280, A = absorbance), indicating that the DNA was sufficiently free from protein.[3] The concentration of DNA was measured using its extinction coefficient (ϵ) at 260 nm after 1:100 dilutions.[4] Stock solutions were stored at 4˚C and used for not more than 4 days. Concentrated stock solutions of the complexes were prepared by dissolving the complexes in DMSO and diluting suitably with the corresponding buffer to the required concentration for all of the measurements.

Absorption spectra titrations were performed at room temperature in Tris HCl/ NaCl buffer (5 mM/ 50 mM buffer, pH 7.4) to investigate the binding affinity between CT-DNA and complex. A fixed concentration of the complex (10 μM) was titrated with increasing amounts of CT-DNA concentration. The intrinsic binding constant for the interaction of complex with CT-DNA was obtained from absorption spectral data.

S3.1.2 Competitive binding experiments

The relative binding of complex to CT-DNA were determined with an DAPI/EB-bound CT-DNA solution in Tris-HCl/ NaCl buffer (5 mM/ 50 mM, pH=7.4). DNA was pre-treated with ethidium bromide for 30 min by maintaining the fixed ratio of [DNA]/ [EtBr or DAPI] = 2.0. The fluorescence quenching effect on addition of complex to the EB-DNA complex have been analysed by recording the fluorescence emission spectra with excitation at 510 nm and emission at 608-610 nm. Similarly, the fluorescence quenching effect on addition of complex to the DAPI-DNA complex have been analysed by recording the fluorescence emission spectra with excitation at 350 nm and emission at 458 nm. The titration quenching experiment was carried out by keeping the concentration of DNA in buffer constant ([CT-DNA] = 10 μM and [dye] = 15 μM) and adding the sample solution within the concentrations range of 0-100 μM. After addition of the sample solution, the solution was kept for 1 min and then fluorescence intensity was measured. The quenching efficiency was calculated from Stern-Volmer (SV) equation.

S3.1.3 Circular dichroism spectral studies

For each spectrum, three scans were collected and the background was subtracted from all of the reagents by using a corresponding solution without CT-DNA as a reference solution (Tris-HCl/ NaCl buffer (5 mM/ 50 mM, pH 7.4)). All CD experiments were performed on a Jasco J-810 spectro-polarimeter at room temperature from 350 to 190 nm.

S3.2 Protein binding study

S3.2.1 Absorption spectral studies

A stock solution of BSA and HSA protein were prepared in TRIS-HCl buffer (pH ~7.4). Concentrated stock solutions of complexes **1** and **2** were prepared by dissolving them separately in TRIS-HCl buffer and diluted suitably to get the required concentrations. An aqueous solution (2 mL) of BSA or HSA protein (10 μM) was titrated by successive additions of the respective

complexes (0-100 μM). Interaction with proteins is also monitored by measuring increment of absorption band at 278 nm in UV-Vis spectroscopy through successive addition of 0-100 μM of **1** and **2** in 10 μM protein solutions.[5]

S3.2.2 Competitive binding experiments

Protein binding studies of the synthesised complexes were carried out by tryptophan fluorescence quenching experiments using human serum albumin (HSA). The excitation wavelength for HSA was at 280 nm, and the quenching of the emission intensity of the tryptophan residues of HSA at 345 nm was monitored using the complexes as a quencher with increased concentration. The excitation and emission slit widths and scan rates were kept constant throughout the experiment. A 10 μM stock solution of HSA was prepared using 50 mM Tris buffer solution and stored at 4 °C for further use. Stock solutions of 5 mM strength were made using synthesized compounds. Fluorometric titration was carried out taking 2 mL of the protein solution and the fluorescence intensity was measured as blank. For titration, each time, a specific amount of the stock solution was added to the protein solution and the fluorescence intensity was measured. For both complexes, solution having concentration range of 0-100 μM was added to measure fluorescence quenching. The quenching efficiency was calculated from Stern-Volmer (SV) equation.

S3.2.3 Viscosity measurements

The viscosity of CT-DNA (100 μM) in the absence and presence of the complexes (with the [complex]/[CT-DNA] ratio of 0, 0.10, 0.20, 0.30, 0.40, 0.50, 0.60, 0.70, 0.80, 0.90 and 1.00) in Tris-HCl buffer (~pH 7.4) was measured using an Ostwald Viscometer at 22 (± 0.1) °C. Each sample was measured in triplicate for accuracy, and the average flow time was determined. Data were presented as $(\eta/\eta_0)^{1/3}$ *versus* [complex]/[DNA], where η_0 and η denote the viscosity of CT-DNA solution in the absence and presence of the complexes, respectively. Viscosity values were calculated according to the relation $\eta = (t_S - t_0)/t_0$, where t_S is the flow time of samples containing CT-DNA and t_0 that of the Tris-HCl buffer alone.[6]

S3.2.4 Circular dichroic spectral studies

Monitoring the far UV-CD spectra (190-250 nm) provides important information to get insight about the change in secondary structure of serum albumin proteins. At first the spectra of free BSA (10 μM) and HSA (10 μM) was recorded and then changes in CD spectra were obtained by

monitoring the binding of metal complexes upon addition of 20 μM of metal complexes successively. For titration, each time, 5 μL of the stock solution was added to the protein solution and the ellipticity (θ) in CD spectra was measured.

S3.2.5 Fourier transform infrared (FTIR) spectroscopic measurements

Infrared spectra were recorded for the solution of complexes treated protein (BSA or HSA) solution which was prepared by constant stirring to ensure the formation of homogeneous solution and to reach the target complex concentration of 0.25 mM with a final protein concentration of 250 μM. Spectra were collected after 2 h incubation of HSA or BSA with solution of complexes at room temperature, using hydrated films. Interferograms were accumulated over the spectral range 4000-500 cm^{-1} with a nominal resolution of 2 cm^{-1} and 32 scans.

S3.3 Molecular modelling

S3.3.1 Molecular Docking

S3.3.1.1 AutoDock simulation method

AutoDock 4.2 MGL tools and Lamarckian Generic algorithm (LGA) were used for proteinfixed ligand-flexible docking calculations. The conformation of complexes was taken from their X-ray crystal structures. A two-step docking protocol was employed to perform the docking experiment. In the first step, both the ligand and protein were extracted in pdb format. The torsion angle and the flexibility issues of the ligand were optimized. For the protein, all the water molecules and the metal ions were removed from the extracted crystal structure. All polar and non-polar hydrogen atoms and the Gasteiger charge were added in to the crystal structure of the protein. In the second step, all possible binding sites of the receptor were determined by the co-crystallized ligand present in the active site of the proteins (for CT-DNA PDB: iz3f, and BSA and HSA having PDB ID of 3V03 and 5K2C). Auto grid version 4.2 was used to calculate the grid parameters and the grid size was set to 40×40×40 points with grid spacing of 0.375 Å. Fifteen search attempts (i.e., ga run parameter) were performed for each compound. The maximum number of energy evaluations before the termination of LGA run was 250,000 and the maximum number of generations of LGA run before termination was 27,000. Other docking parameters were set to the default values of AutoDock 4.2 program. PyMol and software (PyMOL Molecular Graphics System) and Chimera molecular graphics program were used for visualization of the docked pose.[7]

S3.3.2 DFT calculations

The geometry optimization of the ligands was carried out theoretically using Gaussian 09W program package by DFT/B3LYP method as these were unable to produce X-ray diffraction suitable crystals. 6-31G(d,p) basis sets has been chosen through the calculations. All computational processes of ligands were made by using GaussView 5.0.8 software. Here B3LYP stands for Becker's three - parameters exchange functional (B3) in combination with the Lee-Yang-Parr correlation functional (LYP). 6-31G(d,p) is a popular polarized basis set which adds "p" function to hydrogen atoms in addition to the "d" functions on heavy atoms. This basis set uses ECP in calculations.[8]

S3.4 Antibacterial screening

The synthesized Schiff base ligands and their complexes (in 10% (v/v) DMSO) tested against gram negative bacterial strain (Escherichia coli) by agar diffusion method. Initially, the stock cultures were revived by inoculating in broth media and grown at 37 °C for 18 hours with antibiotic disc. The agar plates of the media were prepared and the wells were made in the plate. With 18 hours old cultures each plate was inoculated and spread over the plates. The required concentration of the test sample was introduced into the respective wells. The control wells with gentamycin were also prepared. DMSO at a concentration of 10% and Gentamicin (10 µM per disc) were used as negative and positive controls, respectively for gram-negative bacteria *E-coli*. The plates were incubated at 37 °C for 20 hours. As the organism grows, it forms a turbid layer, except in the region where the concentration of antibacterial agent is above the minimum inhibitory concentration and a zone of inhibition is seen. The size of the inhibition zone depends upon the culture medium, incubation conditions, rate of diffusion and the concentration of the antibacterial agent. The activity was determined by measuring the diameter of zones showing complete inhibition.

S3.5 Cytotoxic assay

The cell line was obtained from the National Centre for Cell Sciences (NCCS) Pune, India. It was cultured in the Dulbecco's Modified Eagles medium (DMEM) supplemented with 10% fetal bovine serum (FBS), 200 mM L-glutamine, 100 µg/mL penicillin, and 10 mg/mL streptomycin in a humidified atmosphere consisting of 5 % CO_2 at 37 ºC. Cells were cultured and maintained in logarithmic growth phase until number of cells reaches at 1.0×10^6 cells/mL.

S3.5.1 Evaluation of cytotoxicity

The cytotoxic effect of complex against cancer cells (MCF-7 and HeLa) was evaluated by MTT [3-(4, 5- dimethylthiazol-2-yl)-2, 5-diphenyl tetrazolium bromide] assay. Briefly, cancer cells were seeded (5 × 104 cells/well) in a 96-well plate and kept in CO_2 for attachment and growth for 24 h. Then, the cells were treated with various concentrations of complex dissolved in DMSO or water (0.25-100 µM) and incubated for 24 h. After incubation, the culture medium was removed and 15 µL of MTT solution (5 mg/mL in PBS) was added to each well. Following 4 h incubation in dark, MTT was discarded and DMSO or water (100 µL/well) was added to solubilize the purple formazan product. The experiment was carried out in triplicates and the medium without complex served as control. The absorbance was measured colorimetrically at 570 nm using an ELISA microplate reader. The percentage of cell viability was calculated using the following formula and expressed as: % cell viability = (OD value of treated cells)/ (OD value of untreated cells (control) × 100.[9] The cytotoxic concentration/ dose that killed 50 % of the cells (IC50) was determined from the absorbance (OD) versus concentration linear regression curve using Prism GraphPad 7 software package.

S3.6 Cell staining assay

4′,6-diamidino-2-phenylindole (DAPI)/ acridine orange (AO) staining was carried out by the method of Gohel et al. Different cancerous cell lines such as A549, HeLa, and MCF-7 were plated at a density of 5×10^4 in 6-well plates. They were allowed to grow at 37°C in a humidified CO_2 incubator until they were 70-80 % confluent. Then cells were treated with various concentrations (including IC_{50} concentration) of ligands and complexes for 24 h. The culture medium was aspirated from each well and cells were gently rinsed thrice with PBS at room temperature. Then equal volumes of cells from control (untreated ligands and complexes) were mixed with 10 µL dye of DAPI/ AO. Finally, the ligand, complex, and dye treated cells were viewed immediately by confocal microscope.

S3.7 Sample preparation for morphological study

The samples containing *E-coli* were fixed using 2.5%/2% glutaraldehyde/ paraformaldehyde in PBS at pH 7.4, and postfixation using 2% tannic acid–guanidine hydrochloride was performed. Similarly, the samples were subject to a third fixation cycle using 2% OsO4. At the end of the fixation procedure, the cells were washed and dehydrated with graded ethanol solutions. Then, the

ethanol solutions were exchanged with graded Freon 113-tf. Finally, the samples were dried in air and AFM data was recorded. Furthermore, the same samples coated with gold were taken for FESEM microscopy.[10]

Precaution! Azide salts are explosive in nature. Proper protections should be taken while using in the laboratory. A very small portion of it was considered during complexation reactions as well as biomedical applications.

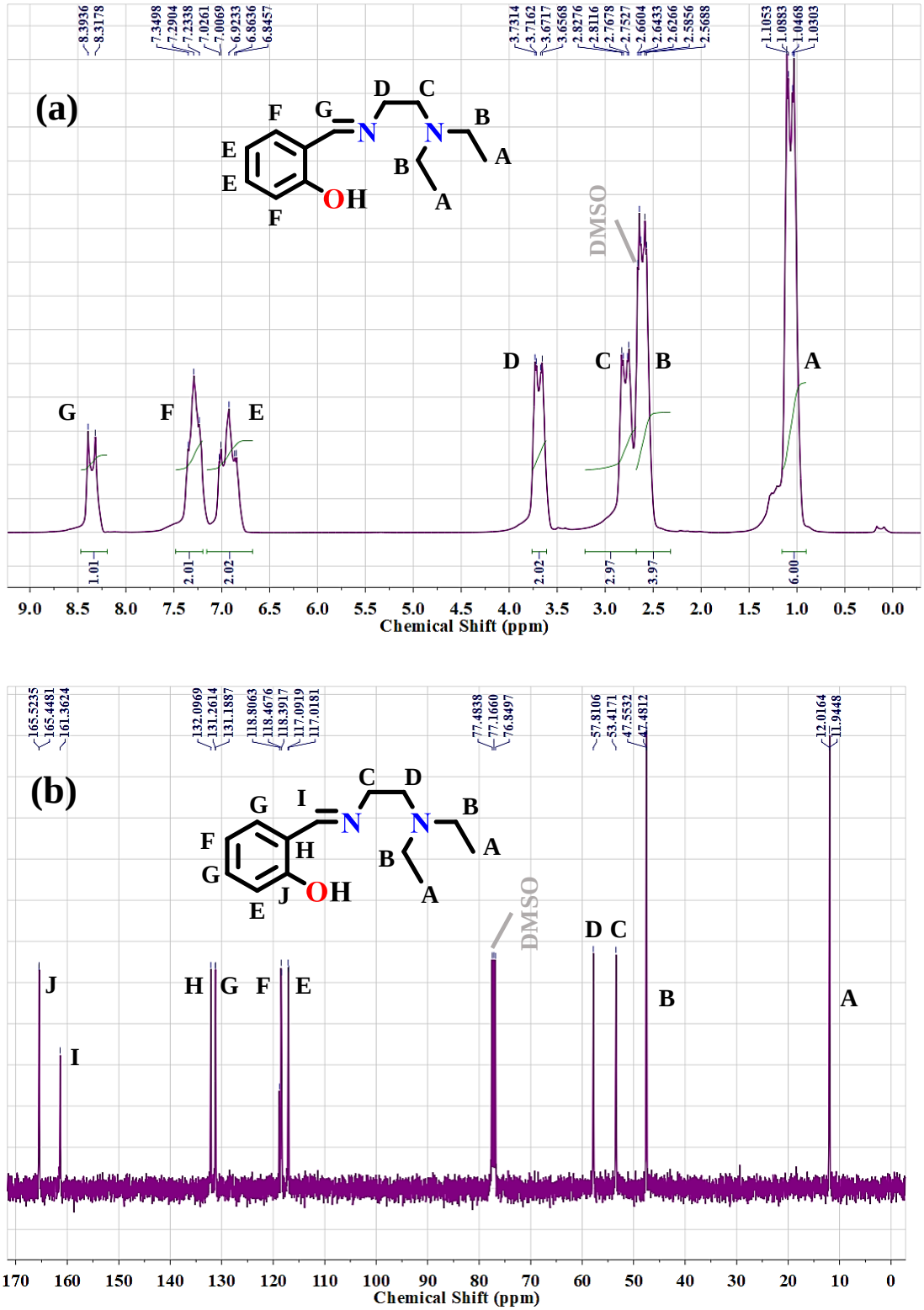

Figure S1. NMR Spectra of ligand **HL[1]** in DMSO-d_6 (400.13 MHz, 298K): (a) ^{1}H NMR and (b) ^{13}C NMR.

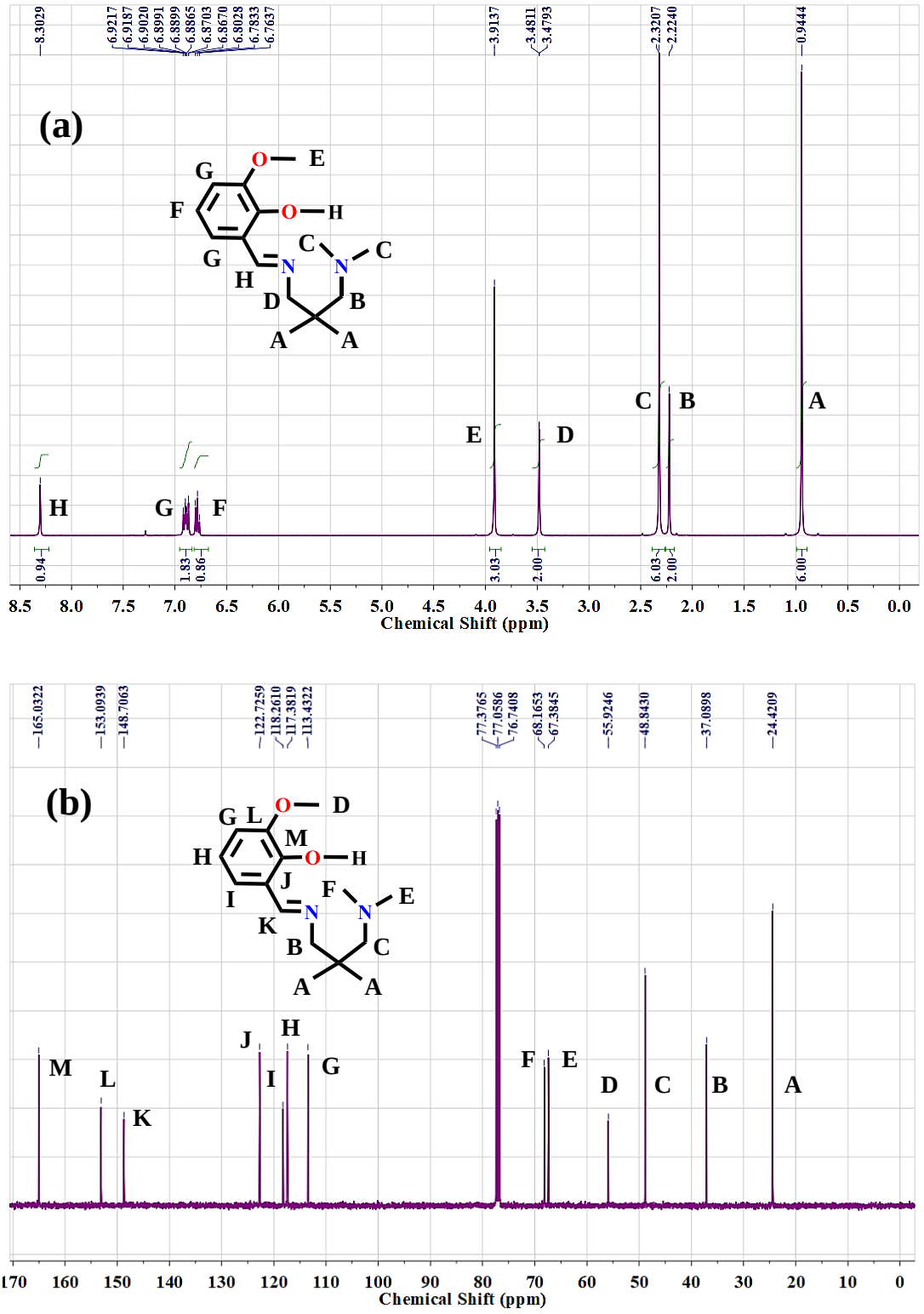

Figure S2. NMR Spectra of ligand **HL²** in DMSO-d_6 (400.13 MHz, 298K): (a) ^{1}H NMR and (b) ^{13}C NMR.

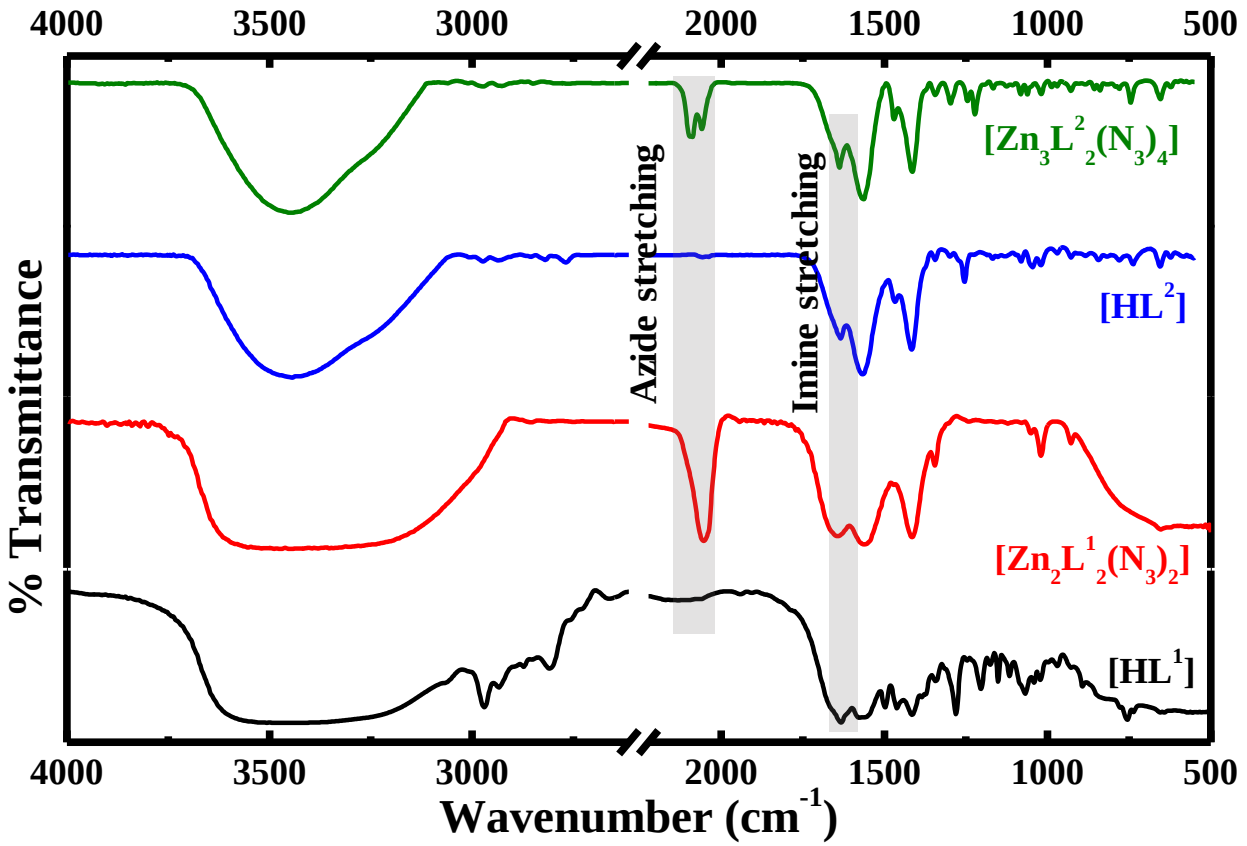

Figure S3. FTIR stretching frequencies of **HL^1**, **HL^2**, **$Zn_2L^1_2(N_3)_2$ (1)** and **$Zn_3L^2_2(N_3)_4$ (2)**. FTIR spectra of complexes **1, 2** show characteristic band for C=N stretching in the region of 1590-1630 cm^{-1}.[11]

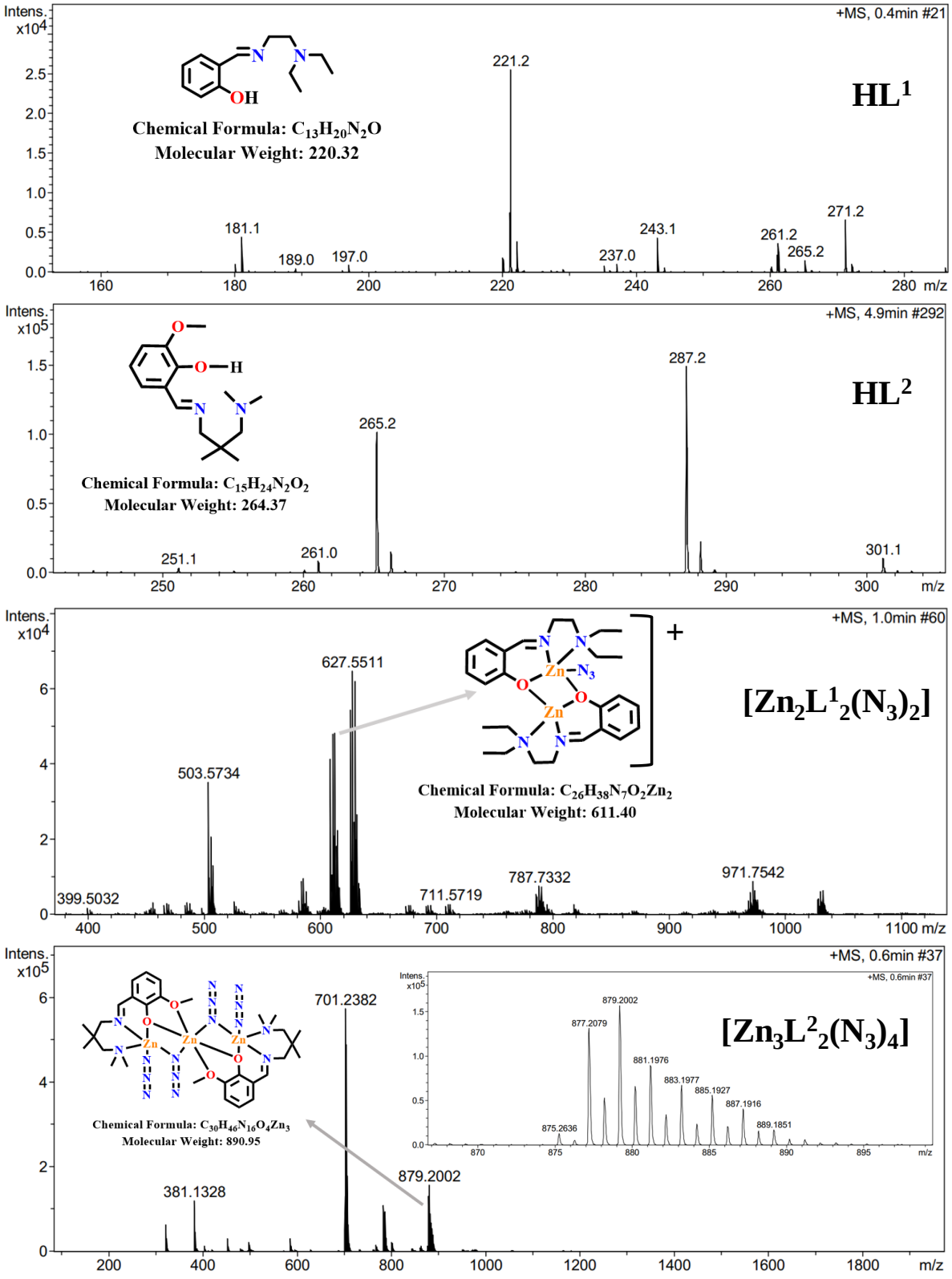

Figure S4. ESI-MS data in HPLC MeOH for **HL**[1], **HL**[2], **1** and **2**.

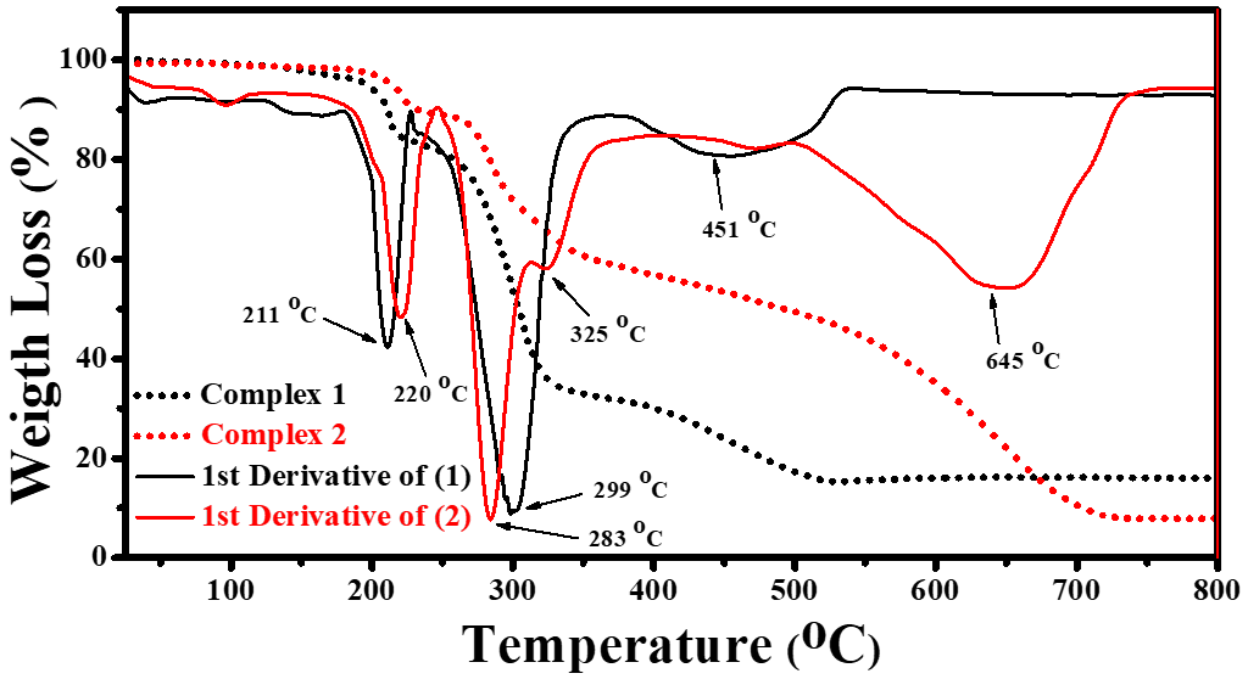

Figure S5. Thermogravimetry analysis (TGA) and their first derivative plots for the complexes **1** and **2**.

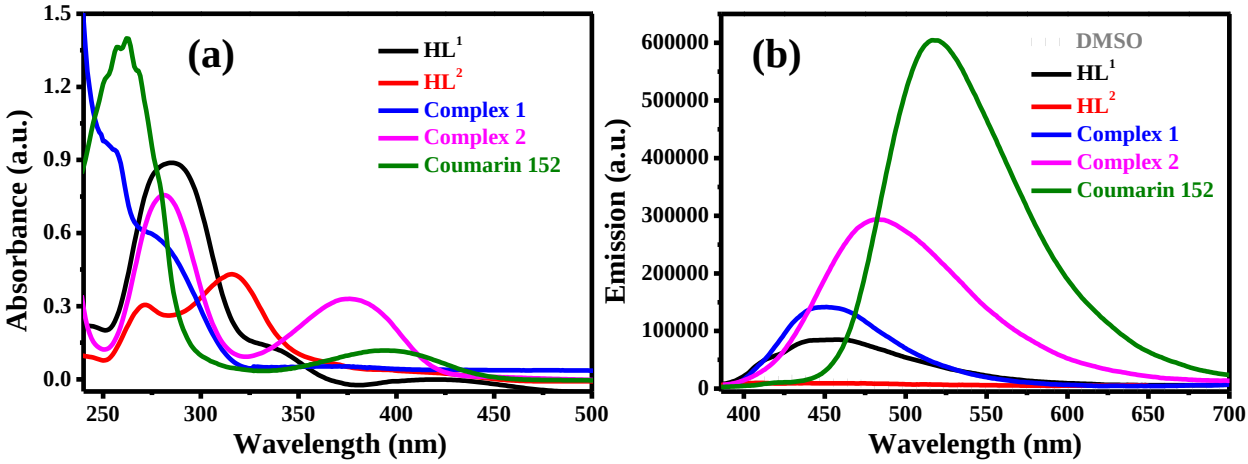

Figure S6. (a) UV-Visible transitions of ligands and complexes (10 μM in HPLC DMSO solvent at 25 °C). (b) Fluorescence emission intensities of the same samples (10 μM in HPLC DMSO solvent at 25 °C). Coumarin 152 has been used as reference for the calculation of quantum yield.

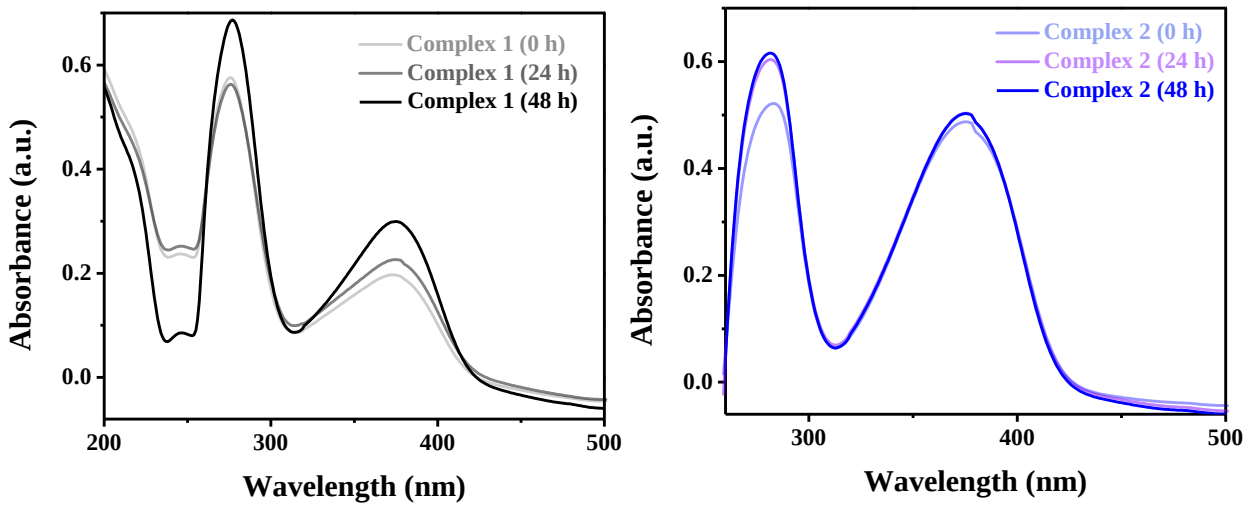

Figure S7. UV-Visible spectra of zinc(II) complexes in 1.5% DMSO in Tris-HCl/NaCl (5 mM/ 50 mM, pH=7.4) buffer mixture over a period of 48 h.

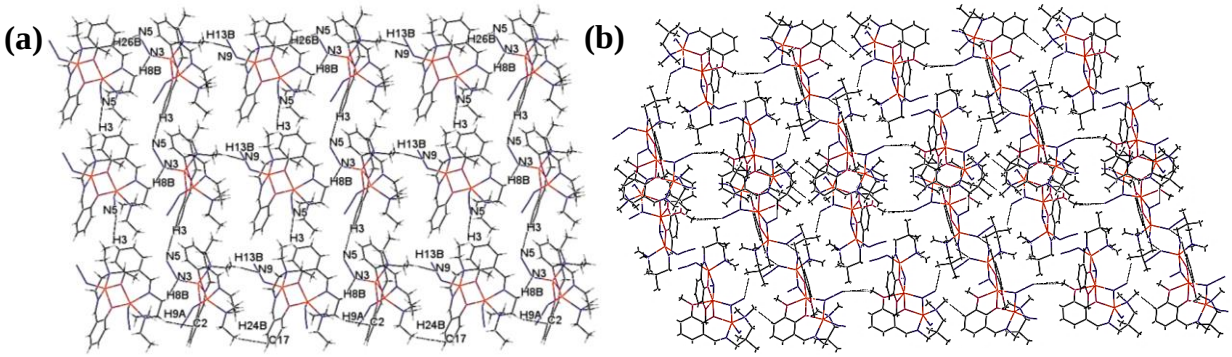

Figure S8. (a) supramolecular framework *via* intermolecular hydrogen bonding for complex **1**, and (b) polymeric extension of complex **2**.

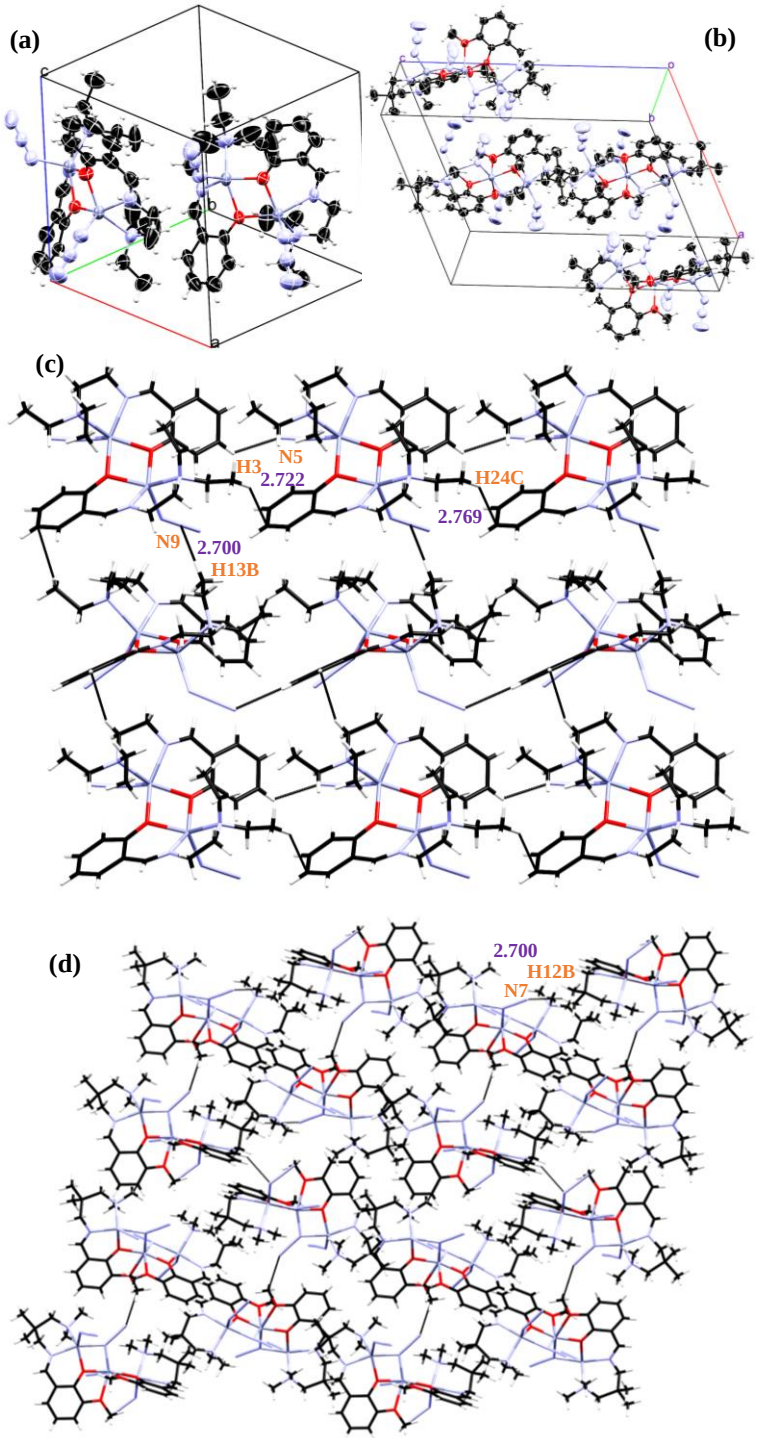

Figure S9. (a) Crystal packing diagram of dimer **1** and (b) trimer **2**. (c) Supramolecular interaction in dimer **1** *via* intermolecular hydrogen bonding (H3…N5, 2.722 Å and H13B…N9, 2.700 Å) and CH…π stacking interaction (2.769 Å). (d) Trimer 2 builds polymeric framework through strong intermolecular hydrogen bonding (H12B…N7, 2.700 Å).

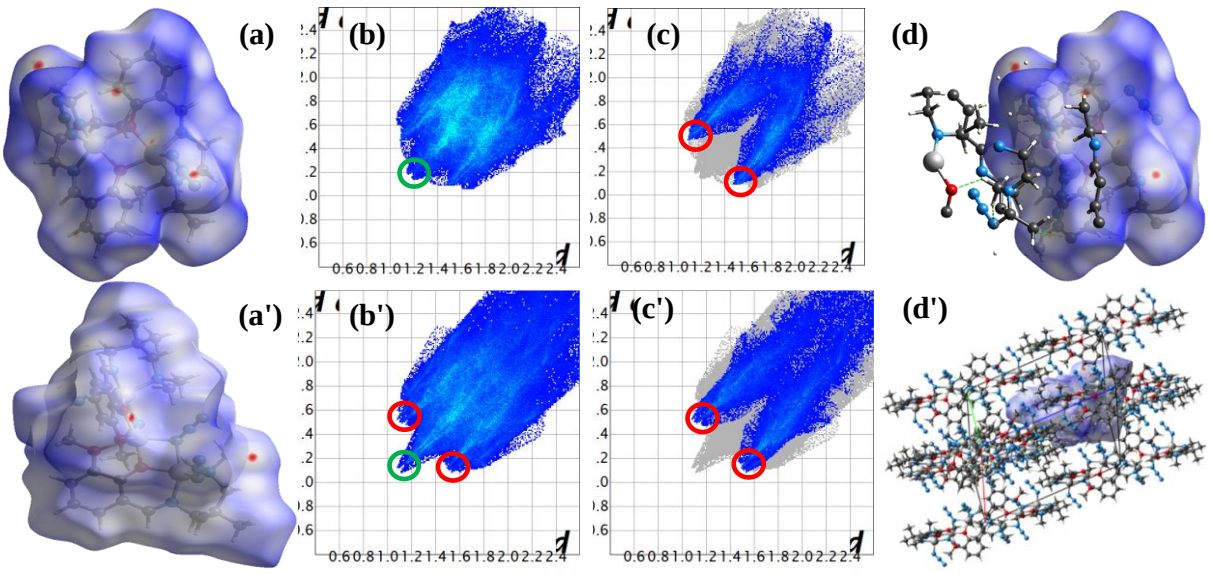

Figure S10. Hirshfeld surfaces mapped with (a-a') d_{norm}, (b-b') associated fingerprint plots and (c-c') strong N…H contacts (31.2% and 34.4% for **1** and **2**, respectively), green rings signify the H...H contacts and (d-d') some selective supramolecular interaction (H-bonds) of the title complexes. Dotted lines (green) represent hydrogen bonds (' denotes the parameters for **2**).

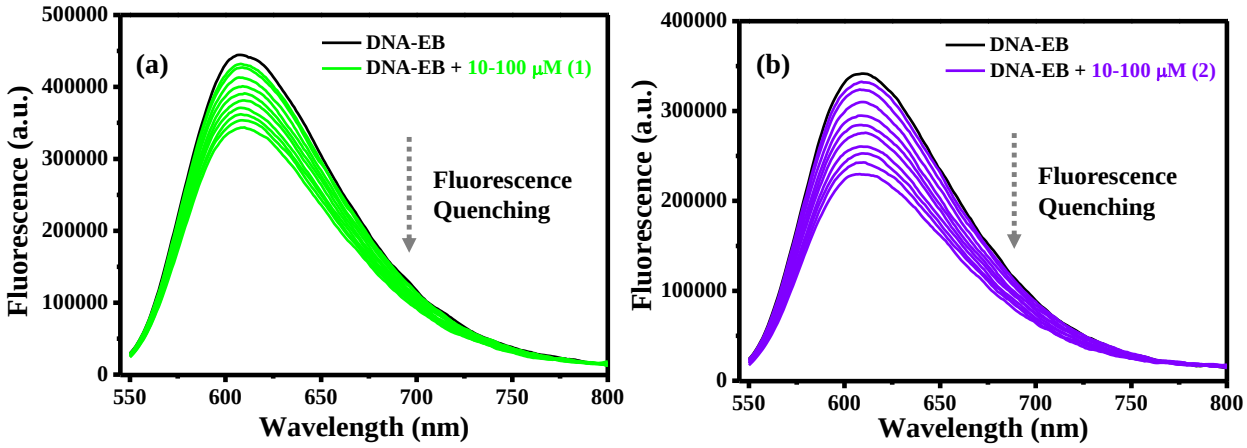

Figure S11. (a) and (b) represents the EtBr displacement assay of complexes **1** and **2**. [DNA] = 10 μM with ethidium bromide (EB 15 μM) and [complex] = 0-100 μM in Tris-HCl/ NaCl buffer (5 mM/ 50 mM, pH=7.4). The arrow shows the fluorescence changes upon increasing the CT-DNA concentration.

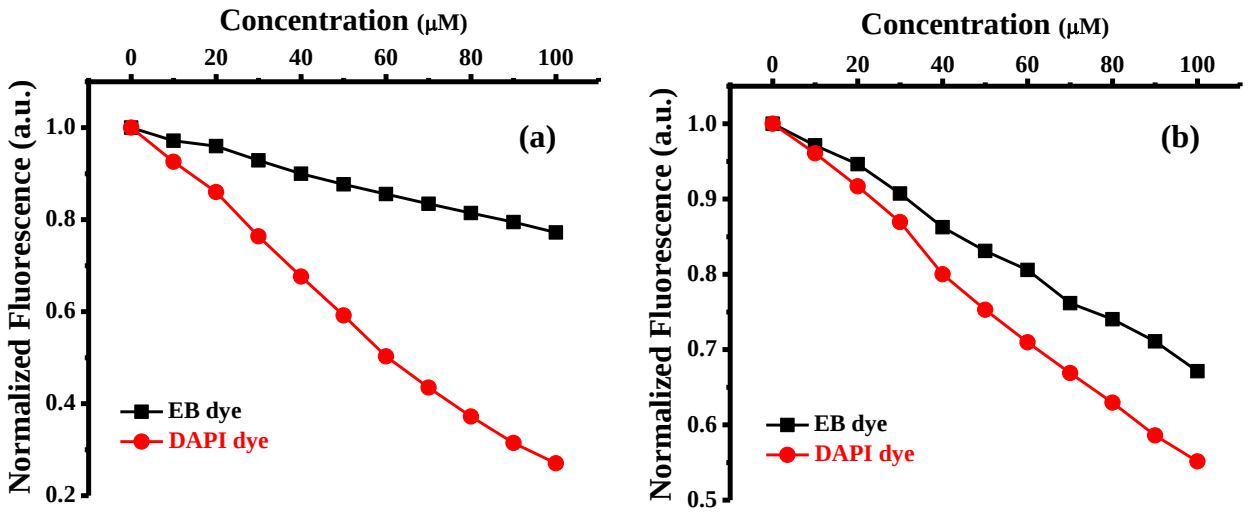

Figure S12. EB versus DAPI displacement assay. Plot of concentration dependent normalized fluorescence by complexes (a) **1** and (b) **2**.

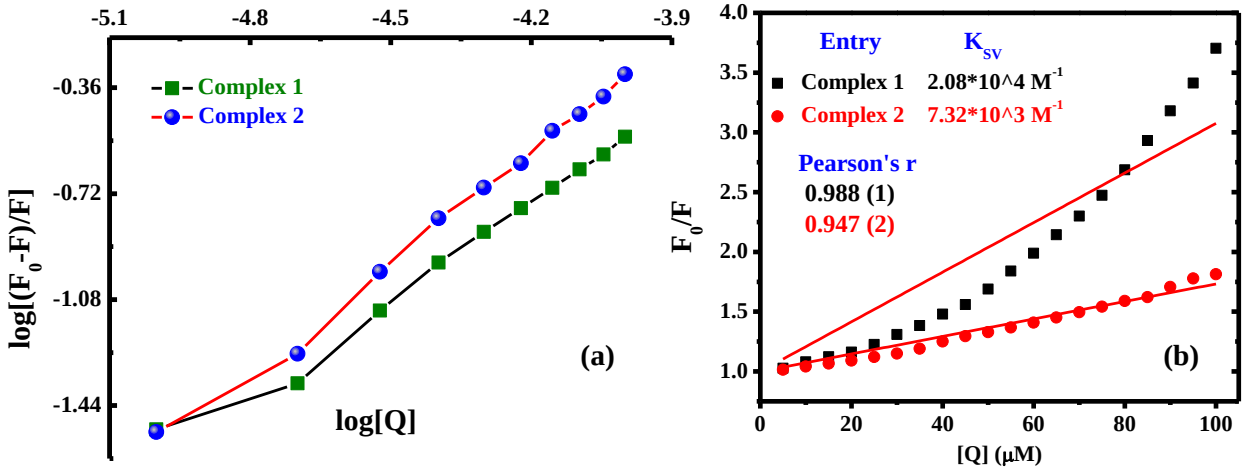

Figure S13. (a) Combine Scatchard plot for the determination of K_a by **1** and **2** *via* EB displacement assay. (b) SV plot to calculate the value of n and K_{sv} *via* DAPI displacement assay.

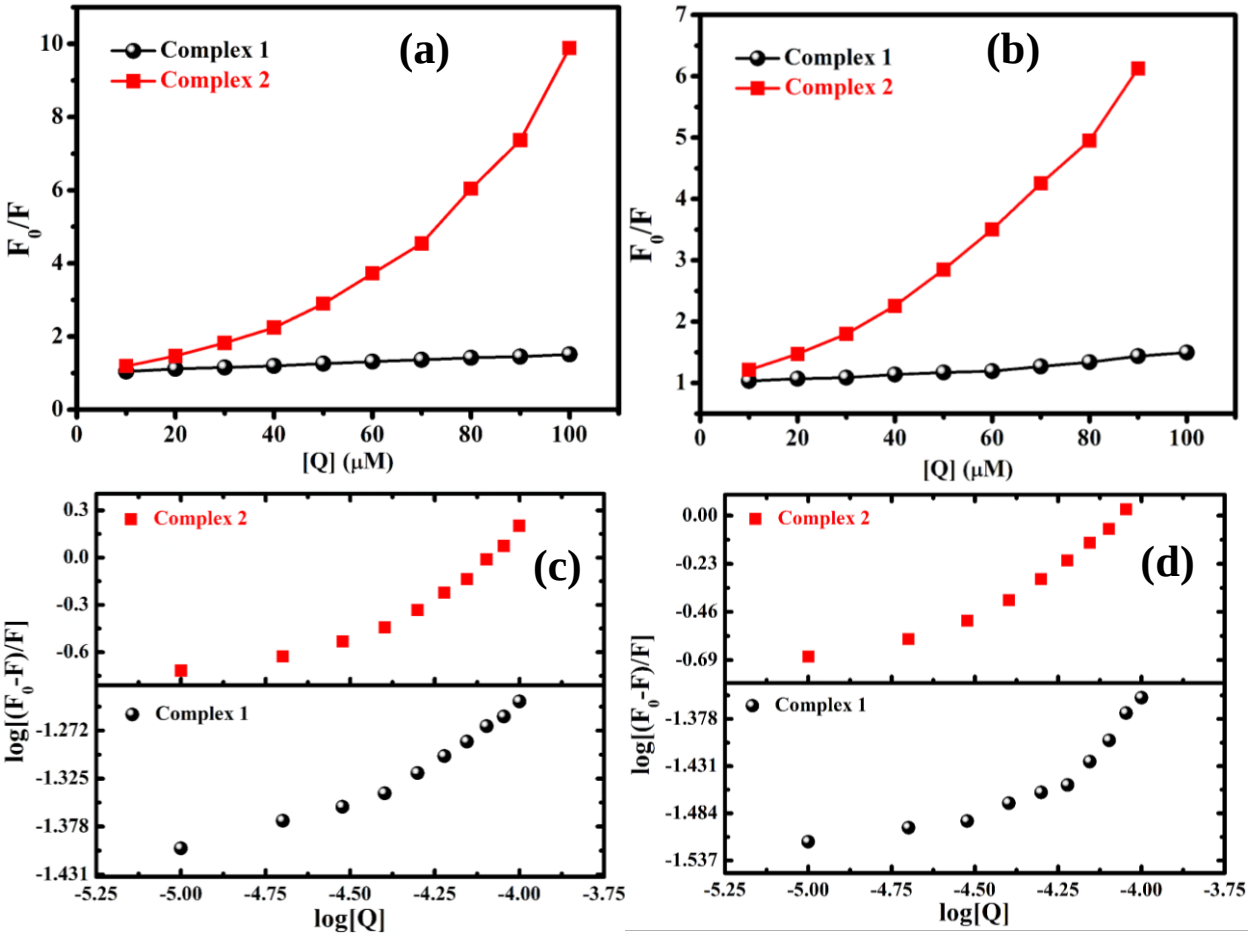

Figure S14. Fluorescence quenching profile by **1** and **2**: (a) Stern-Volmer (SV) plot of BSA. (b) SV plot of HSA. (c) Scatchard plot of BSA. (d) Scatchard plot of HSA.

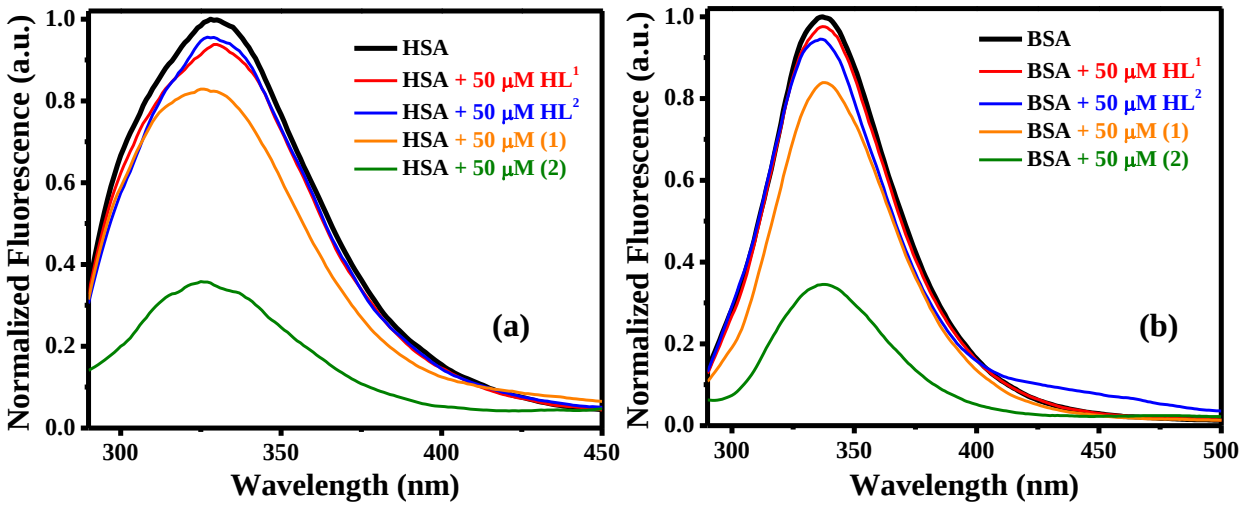

Figure S15. (a) Competitive emission spectra of HSA (10 μM) with 50 μM of ligands and complexes in Tris-HCl/ NaCl buffer (5 mM/ 50 mM, pH=7.4). (b) Similar experiment with BSA.

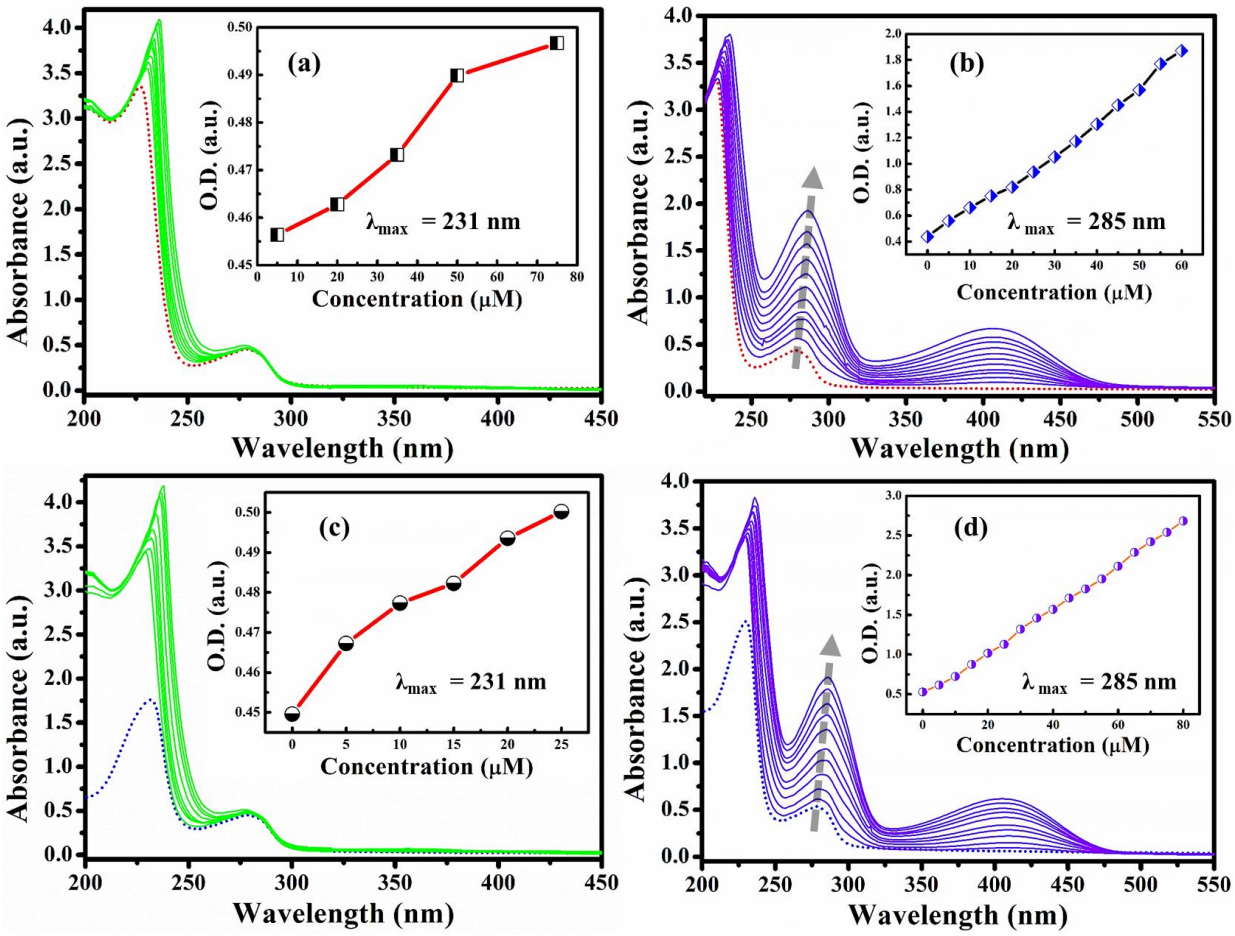

Figure S16. UV-Visible titration diagram of BSA (10 μM) and HSA (10 μM) by successive addition of complex **1** [Graph-(a) and (c)], and complex **2** [Graph-(b) and (d)].

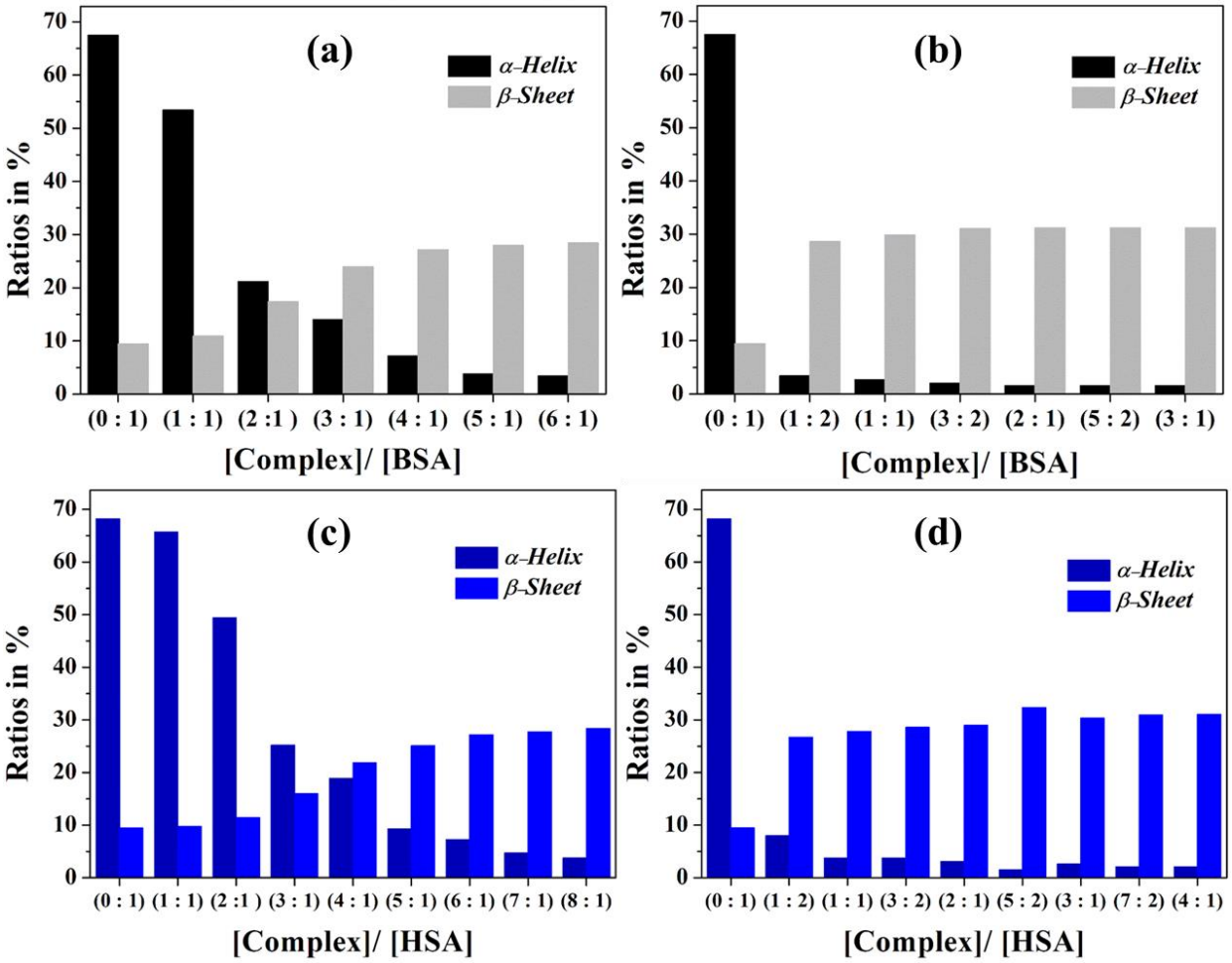

Figure S17. Corresponding histogram of the ratio of different secondary structures of different protein (BSA and HSA) (10 μM) in the absence and presence of **1** and **2** (0-100 μM) at room temperature. (a) and (c) are for complex **1** and (a) and (c) are for complex **2**.

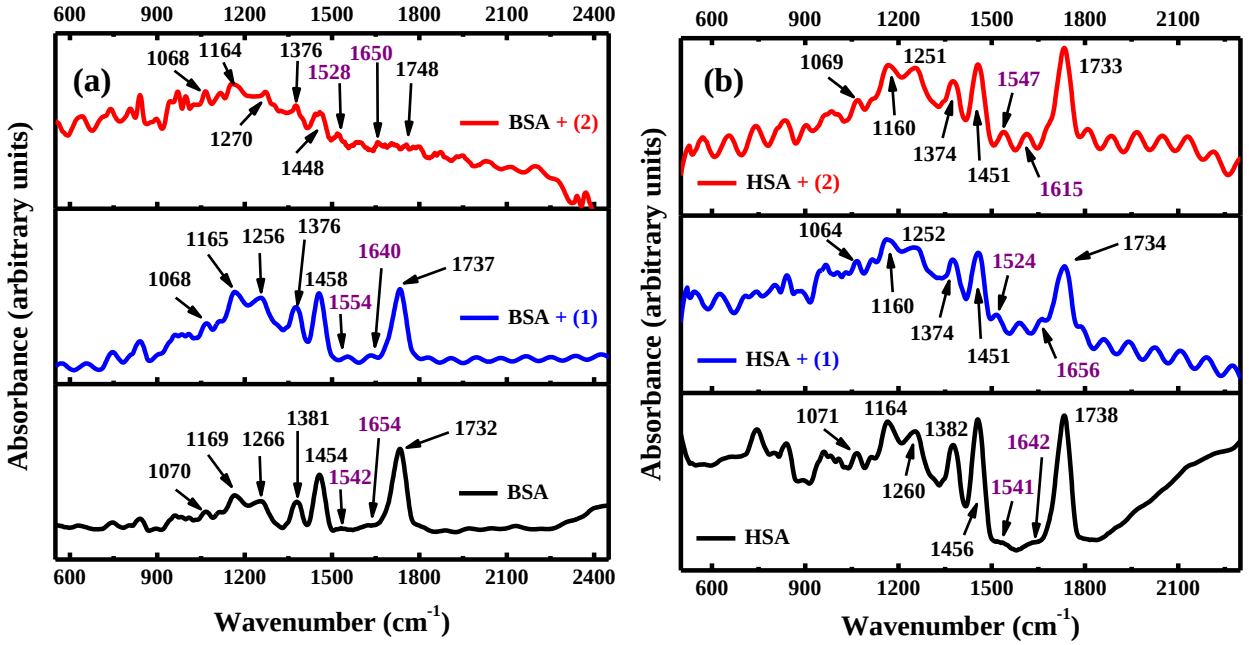

Figure S18. FTIR spectra of complexes treated proteins samples.

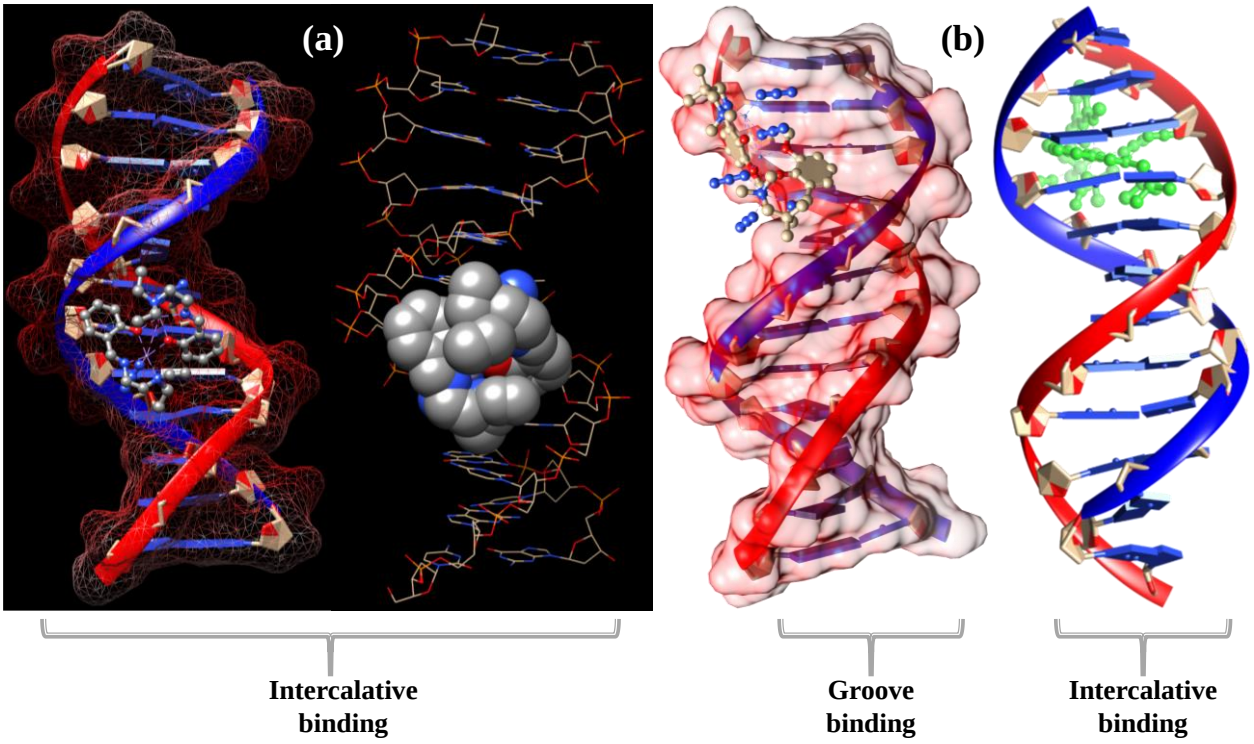

Figure S19. (a) Representation of slight intercalative interaction of dimer **1** with DNA (the hydrophobic surface mesh docking pose). (b) The major groove recognition and intercalation induced distortion of DNA molecule by trimer **2**.

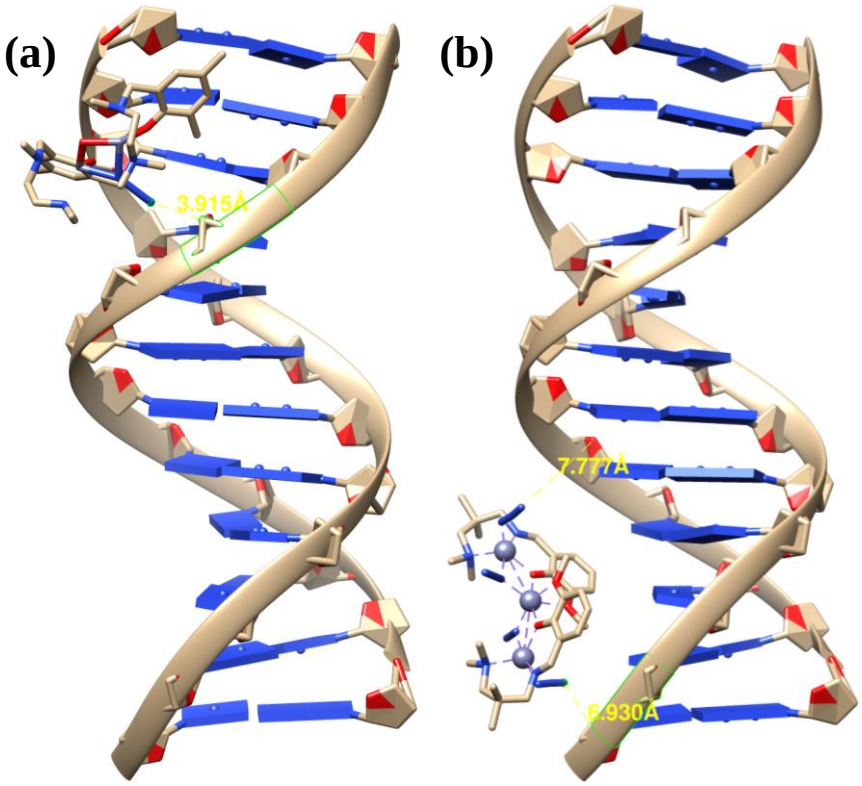

Figure S20. Hydrogen bonding interactions: (a) minor groove binding of dimer **1** and (b) trimer **2** as the major groove binder.

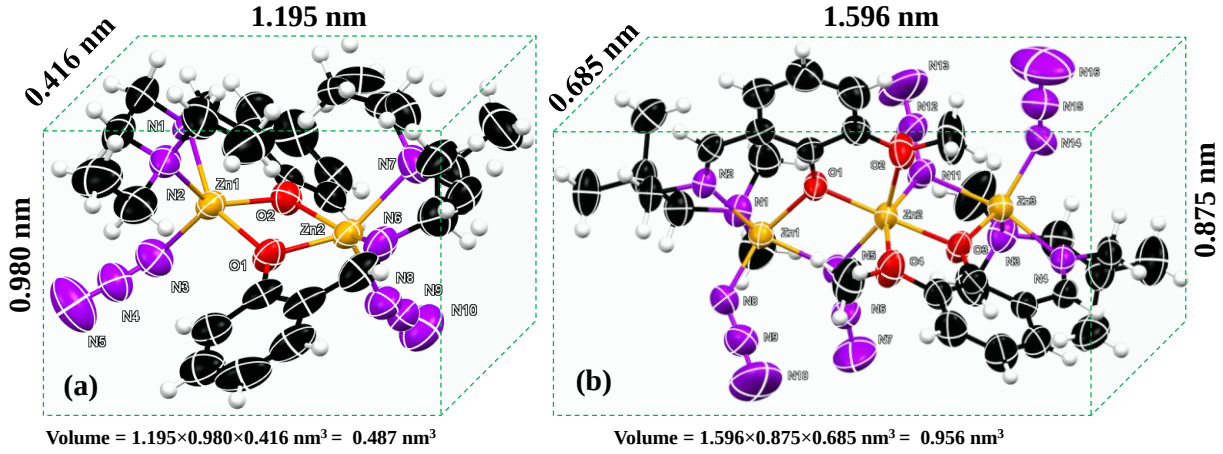

Figure S21. Crystal volume of (a) dimer and (b) trimer, respectively. Here, large volume prefers major groove binding mode.

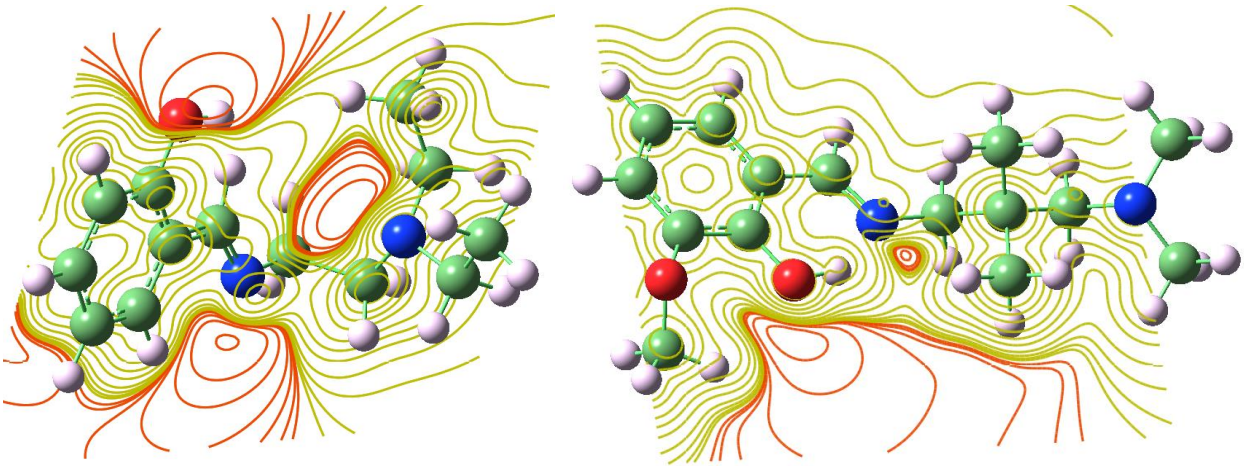

Figure S22. Geometry optimized charged density plots of the ligands.

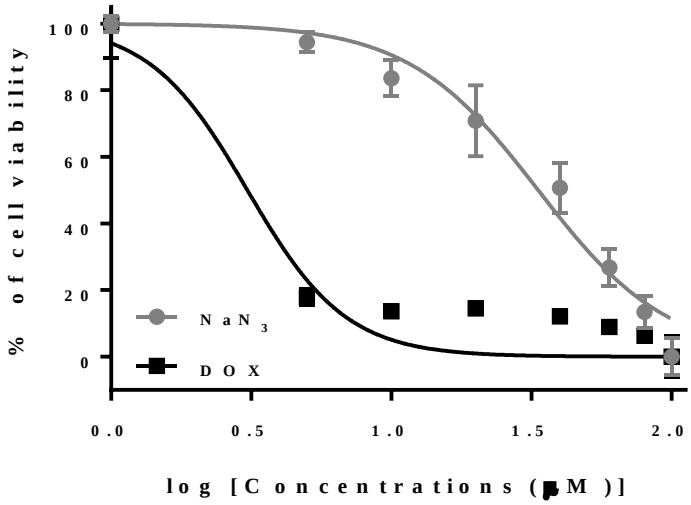

Figure S23. Calculation of IC_{50} values for reference NaN_3 and DOX control against HeLa cancer cell lines.

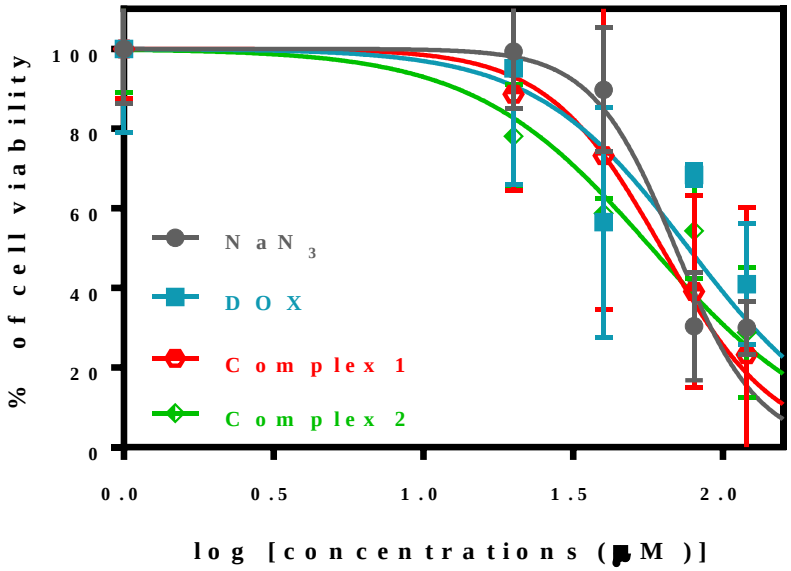

Figure S24. Calculation of IC_{50} values for reference NaN_3, complexes and DOX positive control against human embryonic kidney 293 normal cell (HEK 293) lines.

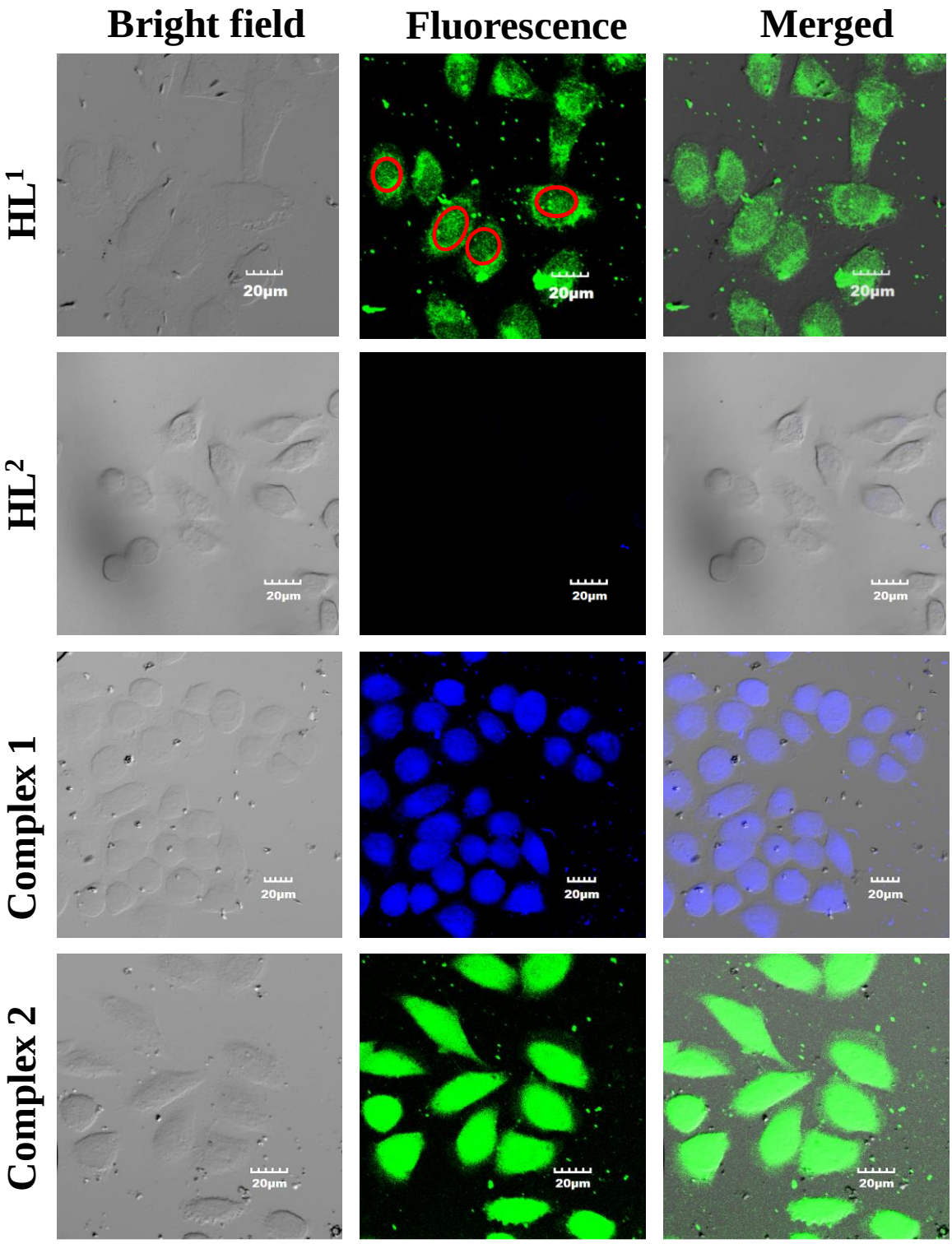

Figure S25. Compounds treated confocal images of HeLa cell lines (10 μM concentration has been used in each cases). Red circles signify the cytoplasm staining ability of **HL[1]**. The scale bar corresponds to 20 μm.

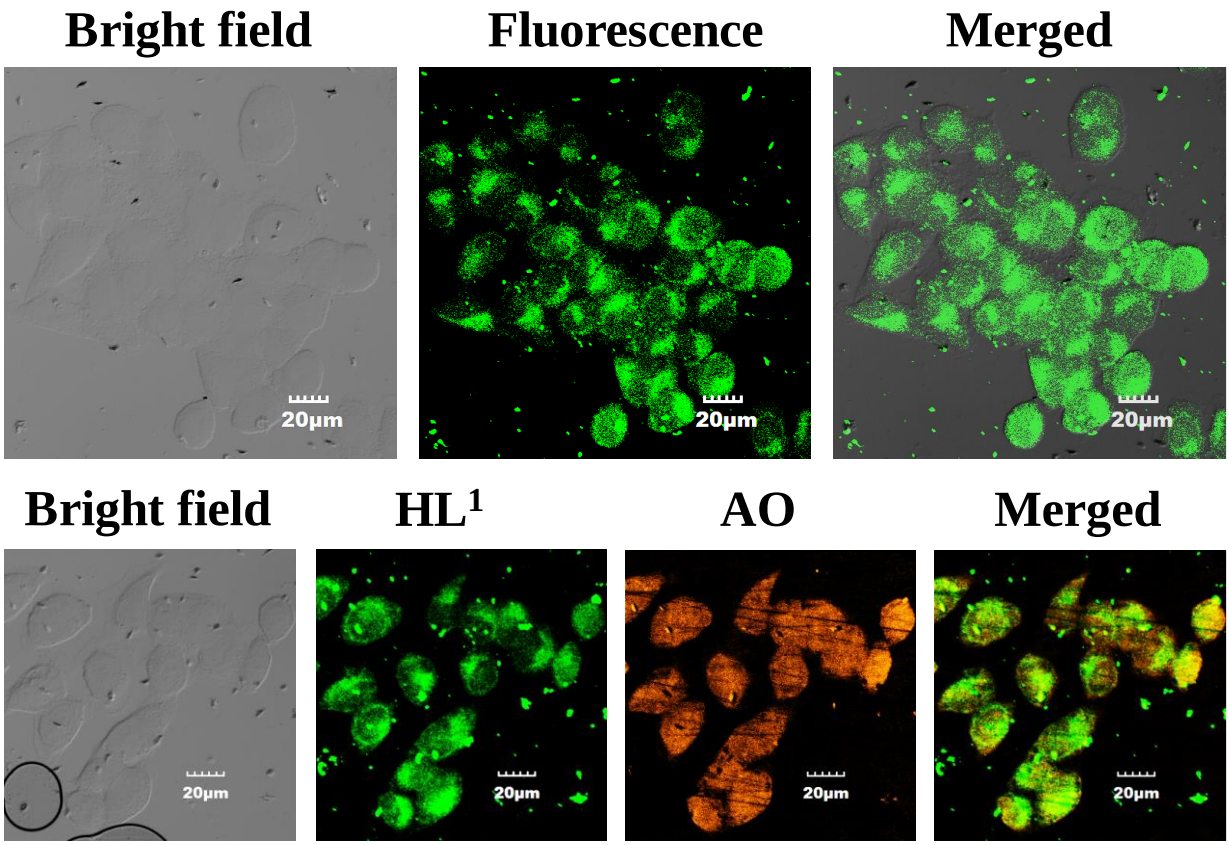

Figure S26. Confocal images of A549 cell lines by 10 μM of **HL^1** (above) showing the visibility on cytoplasm only. AO staining assay to distinguish the unusual imaging behavior of **HL^1** (isolation of nucleus by AO from the rest of the portion of cell (bottom). The scale bar corresponds to 20 μm for each case.

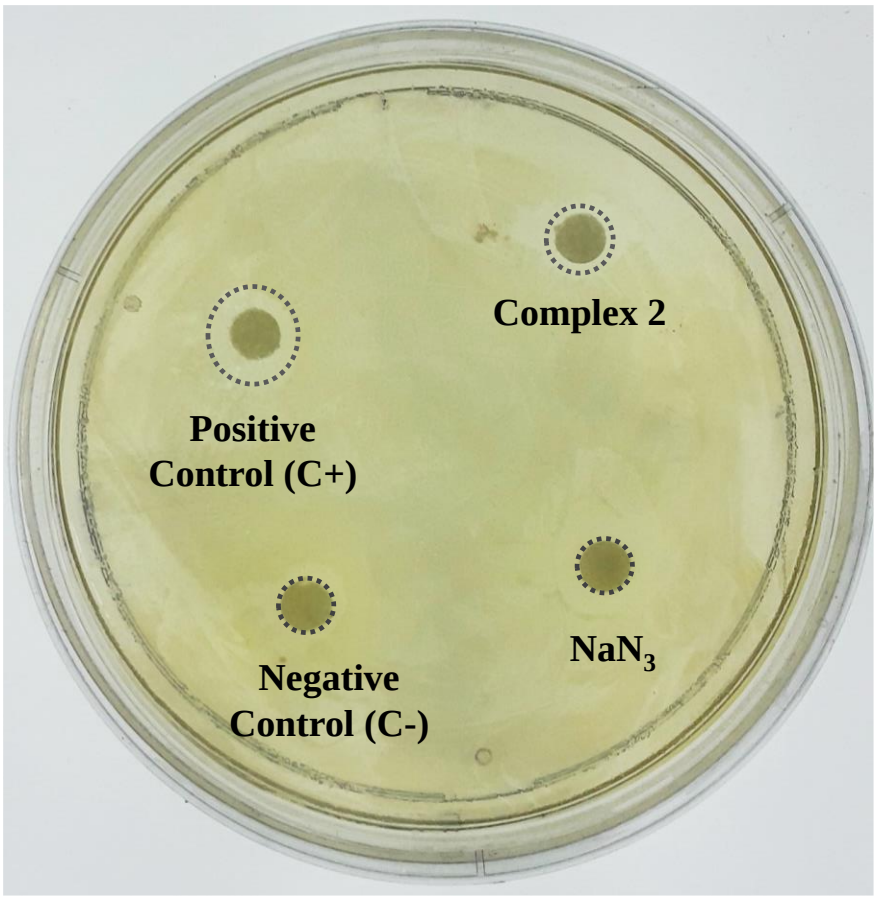

Figure S27. The zone of inhibition against *E-coli* after 24 hours of incubation. DMSO at a concentration of 10% and Gentamicin (5 µM per disc) were used as negative (C-) and positive (C+) controls, respectively for gram-negative bacteria *E-coli*. Moreover, complex **2** and azide salt (5 µM) has been used for comparison.

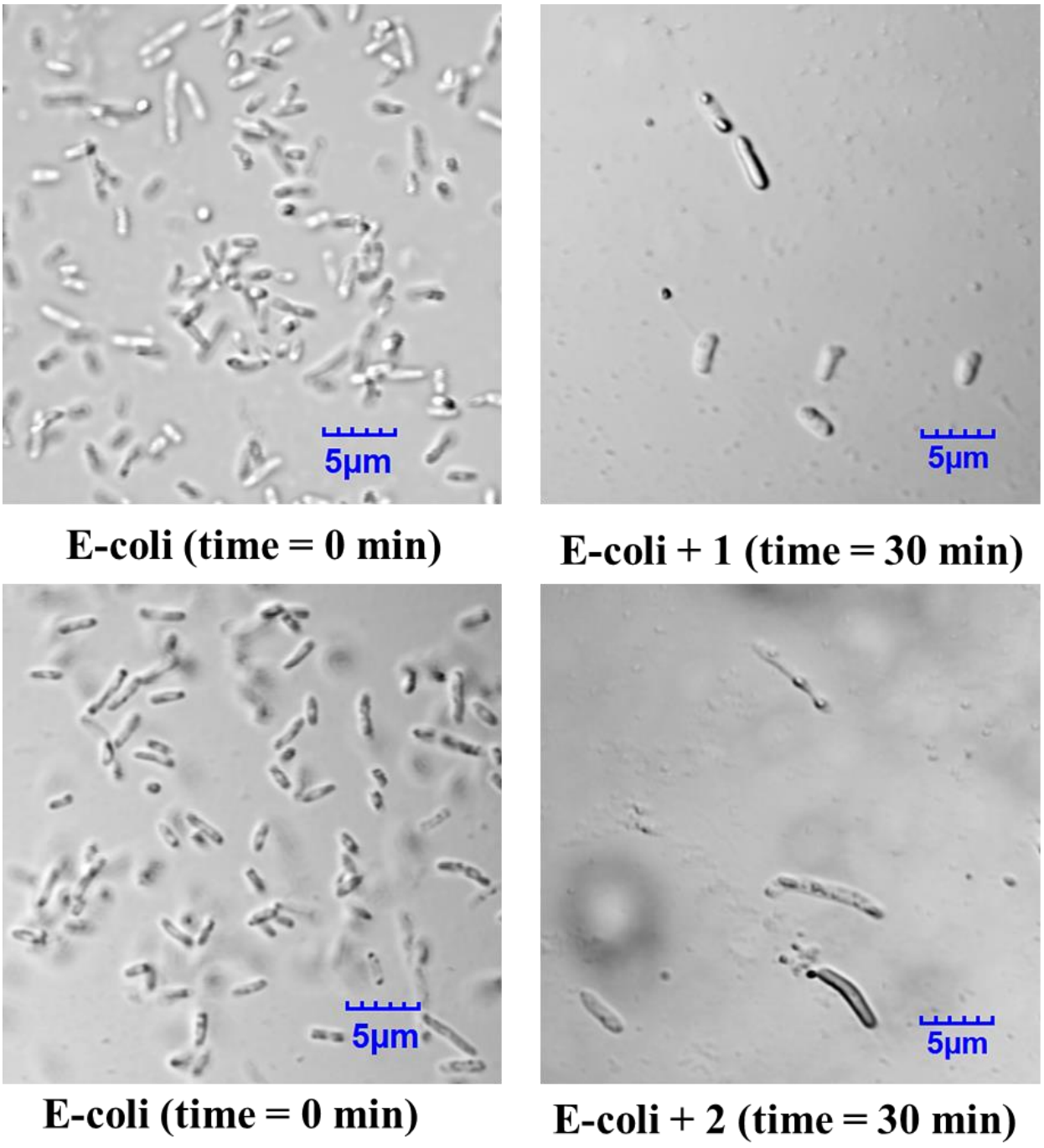

Figure S28. Bright field confocal laser scanning microscopy (CLSM) images of *E-coli* bacterial cells before and after the treatment of the complexes **1** and **2** within 30 min.

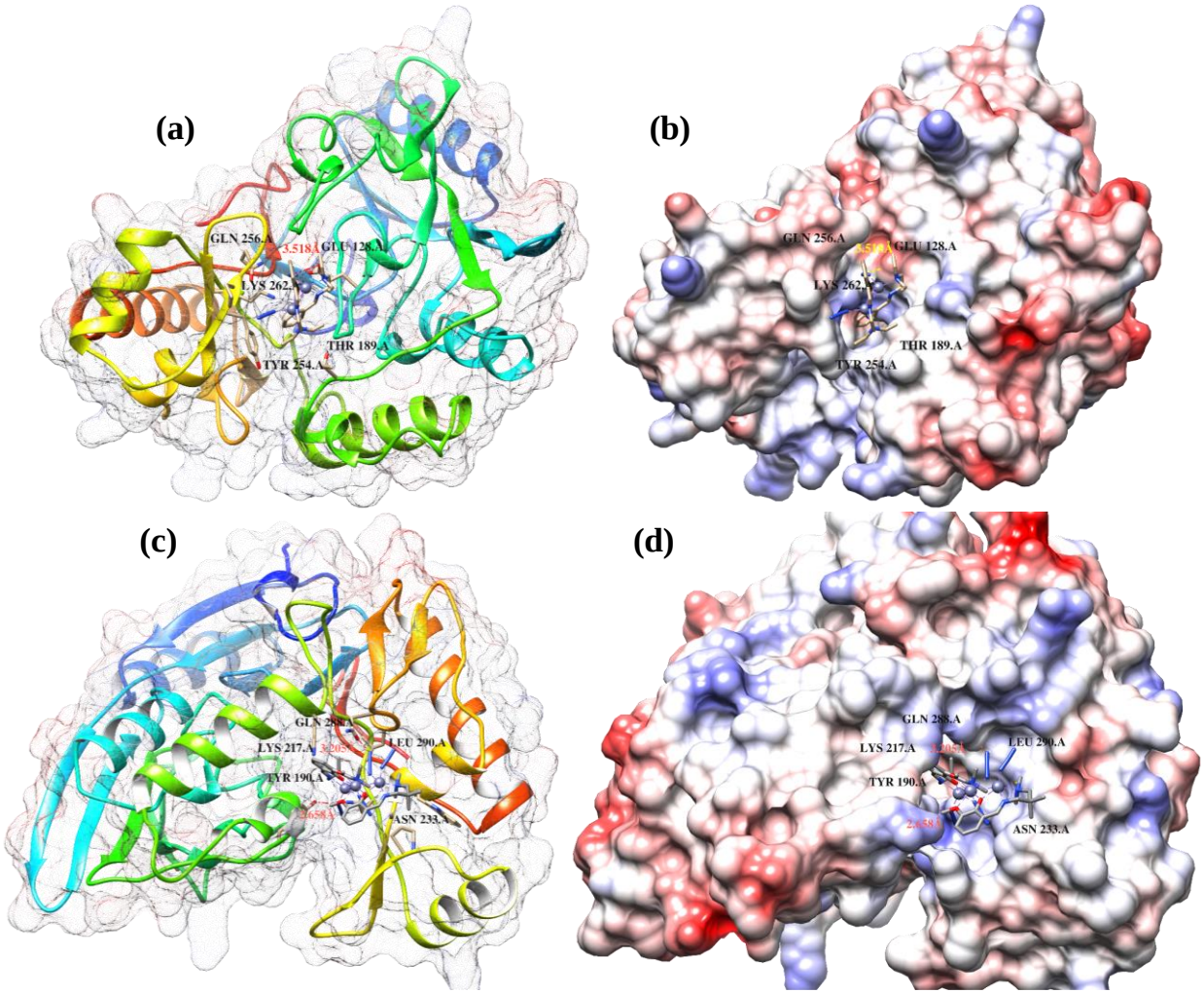

Figure S29. Various docking poses between newly synthesised complexes and the active site of the UDP-N-acetylmuramate dehydrogenase (*E-coli* MurB) enzyme. (a) and (b) are the mesh image and charge balanced (± 15 Kcal/mol) columbic surface colouring diagram for dimer **1** having transparency level of 50%. (c) and (d) represents the similar consequences for trimer **2**.

Table S1. Selected bond lengths (Å) and bond angles (°) of complexes **1** and **2**.

$[Zn_2L^1{}_2(N_3)_2]$ (1)		$[Zn_3L^2{}_2(N_3)_4]$ (2)			
Zn(1)-N(3)	1.990(12)	**Zn(1)-N(1)**	2.1037(17)	**O(4)-Zn(2)-O(2)**	81.32(7)
Zn(1)-O(2)	2.028(8)	**Zn(1)-O(1)**	2.0566(12)	**O(4)-Zn(2)-O(3)**	73.53(5)
Zn(1)-O(1)	2.081(8)	**Zn(1)-N(2)**	2.1059(15)	**N(5)-Zn(2)-O(1)**	79.82(6)
Zn(1)-N(1)	2.091(10)	**Zn(1)-N(5)**	2.1454(17)	**N(5)-Zn(2)-O(2)**	151.69(6)
Zn(1)-N(2)	2.221(11)	**Zn(1)-N(8)**	1.989(2)	**N(5)-Zn(2)-O(3)**	109.05(6)
Zn(2)-N(8)	1.990(12)	**Zn(2)-O(1)**	1.9989(12)	**N(5)-Zn(2)-O(4)**	91.89(8)
Zn(2)-O(1)	2.044(8)	**Zn(2)-O(2)**	2.2977(15)	**N(11)-Zn(2)-O(1)**	111.54(6)
Zn(2)-O(2)	2.079(8)	**Zn(2)-O(3)**	1.9965(13)	**N(11)-Zn(2)-O(2)**	91.88(7)
Zn(2)-N(6)	2.094(11)	**Zn(2)-O4)**	2.2994(16)	**N(11)-Zn(2)-O(3)**	79.42(6)
Zn(2)-N(7)	2.227(11)	**Zn(2)-N(5)**	2.0525(18)	**N(11)-Zn(2)-O(4)**	151.25(6)
N(3)-Zn(1)-O(2)	107.8(5)	**Zn(2)-N(11)**	2.0487(17)	**N(11)-Zn(2)-N(5)**	106.15(8)
N(3)-Zn(1)-O(1)	110.1(4)	**Zn(3)-O(3)**	2.0474(13)	**N(3)-Zn(3)-O(3)**	122.37(7)
O(2)-Zn(1)-O(1)	76.1(3)	**Zn(3)-N(11)**	2.1668(17)	**N(4)-Zn(3)-O(3)**	85.28(6)
N(3)-Zn(1)-N(1)	100.6(5)	**Zn(3)-N(3)**	2.1051(19)	**N(4)-Zn(3)-N(3)**	90.02(7)
O(2)-Zn(1)-N(1)	149.9(4)	**Zn(3)-N(4)**	2.0925(16)	**N(11)-Zn(3)-O(3)**	75.61(6)
O(1)-Zn(1)-N(1)	85.1(4)	**Zn(3)-N(14)**	1.992(2)	**N(11)-Zn(3)-N(3)**	96.54(7)
N(3)-Zn(1)-N(2)	108.2(5)	**N(1)-Zn(1)-O(1)**	114.44(6)	**N(11)-Zn(3)-N(4)**	160.41(6)
O(2)-Zn(1)-N(2)	101.3(4)	**N(2)-Zn(1)-O(1)**	84.36(5)	**N(14)-Zn(3)-O(3)**	132.77(9)
O(1)-Zn(1)-N(2)	140.5(4)	**N(2)-Zn(1)-N(1)**	89.59(6)	**N(14)-Zn(3)-N(3)**	104.73(10)
N(1)-Zn(1)-N(2)	78.6(4)	**N(5)-Zn(1)-O(1)**	76.41(6)	**N(14)-Zn(3)-N(4)**	98.93(8)
N(8)-Zn(2)-O(1)	109.5(5)	**N(5)-Zn(1)-N(1)**	97.90(7)	**N(14)-Zn(3)-N(11)**	97.22(8)
N(8)-Zn(2)-O(2)	111.3(4)	**N(5)-Zn(1)-N(2)**	160.76(6)	**Zn(2)-O(1)-Zn(1)**	104.32(6)
O(1)-Zn(2)-O(2)	75.8(3)	**N(8)-Zn(1)-O(1)**	131.42(8)	**C(1)-O(1)-Zn(1)**	131.43(11)
N(8)-Zn(2)-N(6)	100.2(5)	**N(8)-Zn(1)-N(1)**	114.09(9)	**C(1)-O(1)-Zn(2)**	122.45(11)
O(1)-Zn(2)-N(6)	148.3(4)	**N(8)-Zn(1)-N(2)**	94.00(7)	**C(2)-O(2)-Zn(2)**	112.57(11)
O(2)-Zn(2)-N(6)	83.3(4)	**N(8)-Zn(1)-N(5)**	98.99(8)	**C(11)-O(2)-Zn(2)**	127.48(17)
N(8)-Zn(2)-N(7)	106.7(5)	**O(2)-Zn(2)-O(1)**	73.22(5)	**Zn(3)-O(3)-Zn(2)**	105.47(6)
O(1)-Zn(2)-N(7)	100.9(4)	**O(3)-Zn(2)-O(1)**	164.00(6)	**C(16)-O(3)-Zn(2)**	122.40(12)
O(2)-Zn(2)-N(7)	140.6(4)	**O(3)-Zn(2)-O(2)**	95.40(6)	**C(16)-O(3)-Zn(3)**	131.80(12)
N(6)-Zn(2)-N(7)	80.4(5)	**O(4)-Zn(2)-O(1)**	93.29(6)	**C(17)-O(4)-Zn(2)**	112.20(12)

Table S2. Atomic coordinates (× 10^4) and equivalent isotropic displacement parameters (A^2 × 10^3) for complex **1**. U(eq) is defined as one third of the trace of the orthogonalized Uij tensor.

	x	y	z	U(eq)
Zn(1)	9000(1)	5507(1)	4257(1)	45(1)
Zn(2)	6536(1)	4805(1)	5453(1)	45(1)
O(1)	8457(8)	5214(6)	5953(7)	49(2)
O(2)	7237(8)	4811(8)	3798(7)	51(2)
N(1)	10168(10)	6655(8)	5204(11)	51(3)
N(2)	8838(11)	6712(8)	2820(11)	53(3)
N(3)	10367(12)	4523(10)	3962(11)	62(3)
N(4)	10681(11)	4298(10)	3046(12)	61(3)
N(5)	11070(16)	4102(17)	2157(15)	106(6)
N(6)	4727(10)	5036(9)	4292(11)	58(3)
N(7)	5604(11)	5836(9)	6647(11)	64(3)
N(8)	6294(13)	3392(9)	6024(11)	63(3)
N(9)	6563(11)	2916(10)	6912(12)	57(3)
N(10)	6872(16)	2422(13)	7788(15)	94(5)
C(1)	9240(12)	5261(9)	7031(11)	46(3)
C(2)	9072(13)	4644(10)	8029(11)	53(3)
C(3)	9896(14)	4681(13)	9162(12)	64(4)
C(4)	10942(17)	5357(18)	9381(14)	83(5)
C(5)	11131(15)	5968(15)	8457(14)	74(5)
C(6)	10322(12)	5934(11)	7257(12)	57(3)
C(7)	10638(12)	6645(11)	6350(13)	57(3)
C(8)	10597(16)	7411(13)	4411(15)	73(4)
C(9)	10209(15)	7075(12)	3105(15)	68(4)
C(10)	8614(18)	6271(12)	1510(14)	73(4)

C(11)	8660(20)	7042(15)	482(16)	98(6)
C(12)	7948(16)	7521(13)	2987(19)	82(5)
C(13)	6510(18)	7230(16)	2700(20)	117(8)
C(14)	6633(13)	4405(10)	2755(12)	55(3)
C(15)	7334(15)	3934(11)	1915(12)	60(3)
C(16)	6740(20)	3555(13)	802(15)	77(5)
C(17)	5390(20)	3615(13)	447(16)	87(6)
C(18)	4688(17)	4033(13)	1227(14)	73(5)
C(19)	5253(14)	4422(11)	2393(13)	61(4)
C(20)	4412(14)	4843(13)	3179(14)	67(4)
C(22)	3742(14)	5428(15)	4981(16)	81(5)
C(23)	5800(20)	5447(16)	7886(16)	89(5)
C(24)	5110(20)	5982(17)	8820(20)	112(7)
C(25)	6460(30)	6779(19)	6970(30)	67(9)
C(26)	6840(30)	7300(20)	5920(30)	65(9)
C(25A)	5510(30)	6902(18)	6340(30)	59(8)
C(26A)	6840(30)	7300(30)	6700(40)	77(13)
C(21B)	4380(20)	6211(19)	5900(30)	77(11)
C(21A)	4170(20)	5430(30)	6340(20)	62(11)

Table S3. Atomic coordinates (× 10^4) and equivalent isotropic displacement parameters (A^2 × 10^3) for complex **2**. U(eq) is defined as one third of the trace of the orthogonalized Uij tensor.

	x	y	z	U(eq)
Zn(1)	4342(1)	6511(1)	8656(1)	39(1)
Zn(2)	4866(1)	5934(1)	7439(1)	44(1)
Zn(3)	4974(1)	6732(1)	6105(1)	42(1)
O(1)	5346(1)	5871(1)	8390(1)	44(1)
O(2)	6176(1)	4981(1)	7724(1)	62(1)
O(3)	4468(1)	5570(1)	6515(1)	49(1)
O(4)	4263(1)	4270(1)	7340(1)	64(1)
N(1)	4458(1)	8143(1)	8824(1)	48(1)
N(2)	5237(1)	6247(1)	9590(1)	40(1)
N(3)	4271(1)	8137(2)	5759(1)	58(1)
N(4)	4266(1)	5985(1)	5243(1)	44(1)
N(5)	3802(1)	6564(2)	7635(1)	53(1)
N(6)	3040(1)	6634(2)	7290(1)	62(1)
N(7)	2320(2)	6731(3)	6965(1)	122(1)
N(8)	3304(1)	5854(2)	8815(1)	67(1)
N(9)	2698(1)	5402(2)	8477(1)	68(1)
N(10)	2080(3)	4960(4)	8163(2)	159(2)
N(11)	5423(1)	7149(2)	7105(1)	52(1)
N(12)	6105(2)	7593(2)	7385(1)	72(1)
N(13)	6741(3)	8037(4)	7641(2)	156(2)
N(14)	6150(2)	6915(2)	5985(1)	75(1)
N(15)	6835(2)	6559(2)	6231(1)	79(1)
N(16)	7549(2)	6237(4)	6438(2)	164(2)
C(1)	6061(1)	5300(1)	8712(1)	38(1)
C(2)	6531(1)	4793(2)	8367(1)	47(1)
C(3)	7275(2)	4179(2)	8665(1)	58(1)
C(4)	7570(2)	4057(2)	9323(1)	62(1)

C(5)	7128(1)	4549(2)	9669(1)	52(1)
C(6)	6367(1)	5178(1)	9373(1)	40(1)
C(7)	5947(1)	5682(1)	9777(1)	41(1)
C(8)	4925(2)	6726(2)	10070(1)	49(1)
C(9)	5005(2)	7926(2)	10078(1)	51(1)
C(10)	4395(2)	8437(2)	9454(1)	54(1)
C(11)	6540(3)	4444(3)	7314(1)	111(1)
C(12)	5992(2)	8263(2)	10288(1)	71(1)
C(13)	4617(2)	8308(2)	10583(1)	80(1)
C(14)	5320(2)	8469(2)	8758(1)	68(1)
C(15)	3721(2)	8721(2)	8335(1)	77(1)
C(16)	4042(1)	4680(2)	6284(1)	42(1)
C(17)	3924(2)	3945(2)	6718(1)	51(1)
C(18)	3500(2)	3001(2)	6514(1)	66(1)
C(19)	3166(2)	2775(2)	5865(1)	77(1)
C(20)	3265(2)	3482(2)	5437(1)	65(1)
C(21)	3712(1)	4442(2)	5634(1)	46(1)
C(22)	3832(1)	5124(2)	5153(1)	48(1)
C(23)	4318(2)	6542(2)	4684(1)	53(1)
C(24)	3792(2)	7573(2)	4553(1)	60(1)
C(25)	4185(2)	8383(2)	5091(1)	63(1)
C(26)	4128(3)	3640(3)	7821(1)	88(1)
C(27)	2792(2)	7363(3)	4377(1)	82(1)
C(28)	3947(3)	8077(3)	3972(1)	92(1)
C(29)	3387(2)	8049(3)	5846(2)	86(1)
C(30)	4759(3)	9045(2)	6149(2)	97(1)

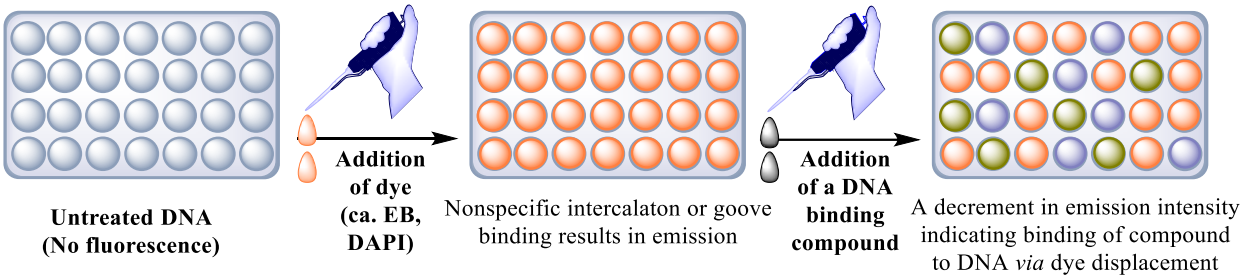

Scheme S1. The dye displacement assay.

References

1. *SAINT V8.34A; Bruker AXS Inc.* **2013**.

2. (a) *SHELXTL -2014/7; Bruker AXS Inc.* **2014**; (b) Dolomanov, O. V.; Bourhis, L. J.; Gildea, R. J.; Howard, J. A.; Puschmann, H., OLEX2: a complete structure solution, refinement and analysis program. *J. Appl. Crystallogr.* **2009,** *42* (2), 339-341.

3. Ganaie, H. A.; Ali, M. N., Short term protocol for the isolation and purification of DNA for molecular analysis. *Int. J. Pharm. Sci. Rev. Res* **2014,** *24* (2).

4. Sunita, M.; Anupama, B.; Ushaiah, B.; Gyana Kumari, C., Synthesis, characterization, DNA binding and cleavage studies of mixed-ligand copper (II) complexes. *Arabian Journal of Chemistry* **2017,** *10*, S3367-S3374.

5. Abeydeera, N.; Perera, I. C.; Perera, T., Synthesis, Characterization, and BSA-Binding Studies of Novel Sulfonated Zinc-Triazine Complexes. *Bioinorganic Chemistry and Applications* **2018,** *2018*, 7.

6. Fu, X.-B.; Liu, D.-D.; Lin, Y.; Hu, W.; Mao, Z.-W.; Le, X.-Y., Water-soluble DNA minor groove binders as potential chemotherapeutic agents: synthesis, characterization, DNA binding and cleavage, antioxidation, cytotoxicity and HSA interactions. *Dalton Transactions* **2014,** *43* (23), 8721-8737.

7. Santos-Martins, D.; Forli, S.; Ramos, M. J.; Olson, A. J., AutoDock4(Zn): an improved AutoDock force field for small-molecule docking to zinc metalloproteins. *J Chem Inf Model* **2014,** *54* (8), 2371-2379.

8. Frisch, M. J.; Trucks, G. W.; Schlegel, H. B.; Scuseria, G. E.; Robb, M. A.; Cheeseman, J. R.; Scalmani, G.; Barone, V.; Petersson, G. A.; Nakatsuji, H.; Li, X.; Caricato, M.; Marenich, A. V.; Bloino, J.; Janesko, B. G.; Gomperts, R.; Mennucci, B.; Hratchian, H. P.; Ortiz, J. V.; Izmaylov, A. F.; Sonnenberg, J. L.; Williams; Ding, F.; Lipparini, F.; Egidi, F.; Goings, J.; Peng, B.; Petrone, A.; Henderson, T.; Ranasinghe, D.; Zakrzewski, V. G.; Gao, J.; Rega, N.; Zheng, G.; Liang, W.; Hada, M.; Ehara, M.; Toyota, K.; Fukuda, R.; Hasegawa, J.; Ishida, M.; Nakajima, T.; Honda, Y.; Kitao, O.; Nakai, H.; Vreven, T.; Throssell, K.; Montgomery Jr., J. A.; Peralta, J. E.; Ogliaro, F.; Bearpark, M. J.; Heyd, J. J.; Brothers, E. N.; Kudin, K. N.; Staroverov, V. N.; Keith, T. A.; Kobayashi, R.; Normand, J.; Raghavachari, K.; Rendell, A. P.; Burant, J. C.; Iyengar, S. S.;

Tomasi, J.; Cossi, M.; Millam, J. M.; Klene, M.; Adamo, C.; Cammi, R.; Ochterski, J. W.; Martin, R. L.; Morokuma, K.; Farkas, O.; Foresman, J. B.; Fox, D. J. *Gaussian 16*, Wallingford, CT, 2016.

9. Sun, J.; Kim, D.-H.; Guo, Y.; Teng, Z.; Li, Y.; Zheng, L.; Zhang, Z.; Larson, A. C.; Lu, G., A c(RGDfE) conjugated multi-functional nanomedicine delivery system for targeted pancreatic cancer therapy. *Journal of Materials Chemistry B* **2015,** *3* (6), 1049-1058.

10. Kundu, B. K. Studies on metal complexes of 'N' O-Donor' ligands in modelling metalloenzymes sensing and catalysis. PhD Thesis, Indian Institute of Technology (IIT) Indore, Indore, 2019.

11. (a) Kundu, B. K.; Das, M.; Ganguly, R.; Bhobe, P. A.; Mukhopadhyay, S., Role of zeolite encapsulated Cu(II) complexes in electron transfer as well as peroxy radical intermediates formation during oxidation of thioanisole. *J. Catal.* **2020,** *389*, 305-316; (b) Kundu, B. K.; Chhabra, V.; Malviya, N.; Ganguly, R.; Mishra, G. S.; Mukhopadhyay, S., Zeolite encapsulated host-guest Cu (II) Schiff base complexes: Superior activity towards oxidation reactions over homogenous catalytic systems. *Microporous Mesoporous Materials* **2018,** *271*, 100-117.